

Field distribution analysis in deflecting structures.

V.V. Paramonov

Institute for Nuclear Research, 117312, Moscow, Russia

Abstract

Deflecting structures are used now mainly for bunch rotation in emittance exchange concepts, bunch diagnostics and to increase the luminosity. The bunch rotation is a transformation of a particles distribution in the six dimensional phase space. Together with the expected transformations, deflecting structures introduce distortions due to particularities - aberrations - in the deflecting field distribution. The distributions of deflecting fields are considered with respect to non linear additions, which provide emittance deteriorations during a transformation. The deflecting field is treated as combination of hybrid waves HE_1 and HM_1 . The criteria for selection and formation of deflecting structures with minimized level of aberrations are formulated and applied to known structures. Results of the study are confirmed by comparison with results of numerical simulations.

Contents

1	Introduction	3
2	Field description	3
2.1	Relations between field components	4
2.2	Properties of Bessel functions	5
2.3	Field components of dipole mode	5
2.4	Basis problem. Hybrid waves HE , HM	6
2.5	Supporting structure	8
3	Deflecting field representation and analysis	9
3.1	Synchronous spatial harmonic	9
3.2	Higher spatial harmonics for dipole mode	11
3.3	Multipole additions	12
3.4	Bunch deflection and bunch rotation	13
3.5	Criterion for higher harmonics estimation in periodical structures	14
3.6	Panofsky-Wenzel theorem	15
4	Traveling and standing wave operation	16
4.1	Deflecting field distributions for TW and SW mode	17
4.2	Phase deviations in deflecting field distribution	20
4.3	RF efficiency for TW and SW mode	21
5	Parameters of the DLW structure	22
5.1	Parameters for TW mode	23
5.2	Parameters for SW mode	25
6	Parameters of the decoupled TE-structure	25
6.1	Parameters for TW mode	27
6.2	Parameters for SW mode	28
7	Hybrid waves phasing and balance.	29
7.1	Structures classification	32
8	End cell problem	33
8.1	End cell for SW mode	33
8.2	End cell for TW mode	34
9	Dispersion properties and limitations	36
10	Summary	38
11	Acknowledgments	38
	References	39

1 Introduction

In particle accelerators Deflecting Structures (DS) - periodical structures with transverse components of the electromagnetic field at the axis - were introduced for charged particle deflection and separation. A bunch of charged particles crosses a DS synchronously with the maximal deflecting field Ed , corresponding to a phase $\phi = 0$ in the structure, and particles get an increment in the transverse momentum p_t . It allows both to deflect particles from the axis and to separate particles with different charge and momentum in space, see, for example, [1].

In the modern facilities with short and bright bunches DS found other applications, such as short bunch rotation for special diagnostics, emittance exchange experiments and luminosity enhancement. All these applications are related to the transformation of particle distributions in the six dimensional phase space. For these applications the DS operates in another mode - the center of the bunch crosses the DS at zero value of E_d , corresponding to $\phi = \frac{\pi}{2}$, see, for example [2].

The applications for particle distribution transformations provide additional specific requirements. Usual RF parameters, like RF efficiency, field rise time, total deflecting voltage V_d , describe general parameters - achievable resolution of measurements, possibility for single bunch measurements in the bunch train and the price for this with respect to the RF system.

But, together with the expected transformations, DS provide distortions due to particularities in the deflecting field distribution. The tool for distribution transformation should provide as minimal as possible intrinsic distortions.

In a complicated DS geometry the distribution of the electromagnetic field components can be obtained with good precision only in numerical simulations. And the distortions of particle distributions can be estimated quantitatively also only in numerical simulations of the beam dynamics.

As it is known from theory, a system with linear spatial distribution of the field components doesn't change the bunch emittance. To avoid multiple coupled simulations of field distributions and particle dynamics for different possible DS solutions and bunch parameters, we investigate first the different DS options for criteria of field linearity, i.e. minimal deviations from a linear field distribution.

2 Field description

In the periodical structure the field distribution for each j -th component $E_j(\vartheta, r, z)$ can be represented in complex form and satisfies the Floquet theorem:

$$\begin{aligned} E_j(\vartheta, r, z) &= E_j(\widehat{\vartheta}, r, z) e^{i\psi_j(\vartheta, r, z)} \quad -d/2 \leq z < d/2, \\ E_j(\vartheta, r, z + nd) &= E_j(\widehat{\vartheta}, r, z) e^{i(\psi_j(\vartheta, r, z) - n\Theta_0)}, \quad 0 \leq \Theta_0 \leq \pi, \end{aligned} \quad (1)$$

where $E_j(\widehat{\vartheta}, r, z)$ and $\psi_j(\vartheta, r, z)$ are the amplitude and the phase distributions of the field components at the period, correspondingly, d is the period length, Θ_0 is the phase advance per period, and n is the period number.

If the structure has a planes of mirror symmetry (the mostly realized case in practice), $E_j(\widehat{\vartheta}, r, z)$ is all time an **even** function with respect to the mirror plane and $\psi_j(\vartheta, r, z)$ is an **odd** function with a possible total shift at $\pi/2$ or π .

In the beam aperture of a slow wave structure the field components can be expanded, see for

example [3], into a Fourier series over the spatial harmonics:

$$E_j(\vartheta, r, z) = \sum_{p \rightarrow -\infty}^{p \rightarrow +\infty} a_{jp}(\vartheta, r) e^{-ik_{zp}z}, \quad k_{zp} = \frac{\Theta_0 + 2p\pi}{d}, \quad p = 0, \pm 1, \pm 2, \dots, \pm \infty \quad (2)$$

with

$$a_{jp}(\vartheta, r) = \frac{1}{d} \int_{-\frac{d}{2}}^{\frac{d}{2}} E_j(\vartheta, r, z) e^{ik_{zp}z} dz. \quad (3)$$

where $a_{jp}(\vartheta, r)$ and k_{zp} are the amplitude and wave number of the p -th spatial harmonic, respectively. Taking into account parity properties for the amplitude and the phase in (2), the functions $a_{jp}(\vartheta, r)$ in (2) are either real or imaginary.

To avoid the additional introduction of symbols, below we will use and assume the symbols for spatial harmonics in two options. If the symbol $a_{jp}(\vartheta, r)$ is used, it means the function with respect ϑ, r , including the constant amplitude coefficient. And the symbol a_{jp} , without dependence on the coordinates, means the constant amplitude coefficient for respective spatial harmonic.

For the slow wave system the spatial harmonics in the field representation (2) are necessary for the boundary conditions at the aperture radius $r = a$. In the aperture volume both total field and each spatial harmonic should satisfy to the Maxwell equations.

2.1 Relations between field components

For the complete description of the field distribution two independent variables are required. For structures periodical in z it is common practice to consider the longitudinal components E_z and H_z as such independent variables.

From Maxwell equations

$$\text{rot} \vec{H} = \frac{\partial \vec{D}}{\partial t}, \quad \text{rot} \vec{E} = -\frac{\partial \vec{B}}{\partial t}, \quad \text{div} \vec{B} = 0, \quad \text{div} \vec{D} = 0, \quad \vec{D} = \epsilon_0 \epsilon \vec{E}, \quad \vec{B} = \mu_0 \mu \vec{H}, \quad (4)$$

and assuming a $\sim e^{i\omega t}$ time dependence in vacuum, i.e. $\epsilon = \mu = 1$, one can get in cylindrical coordinates r, ϑ, z :

$$\begin{aligned} \frac{\partial^2 E_r}{\partial z^2} + k^2 E_r &= \frac{\partial^2 E_z}{\partial r \partial z} - \frac{iknZ_0}{r} H_z, \\ \frac{\partial^2 E_\vartheta}{\partial z^2} + k^2 E_\vartheta &= -\frac{n}{r} \frac{\partial E_z}{\partial z} + ikZ_0 \frac{\partial H_z}{\partial r}, \\ Z_0 \frac{\partial^2 H_r}{\partial z^2} + k^2 Z_0 H_r &= -\frac{ikn}{r} E_z + Z_0 \frac{\partial^2 H_z}{\partial r \partial z}, \\ Z_0 \frac{\partial^2 H_\vartheta}{\partial z^2} + k^2 Z_0 H_\vartheta &= -ik \frac{\partial E_z}{\partial r} + \frac{nZ_0}{r} \frac{\partial H_z}{\partial z}, \end{aligned} \quad (5)$$

where

$$k = \frac{\omega}{c} = \omega \sqrt{\epsilon_0 \mu_0}, \quad Z_0 = \sqrt{\frac{\mu_0}{\epsilon_0}}, \quad (E_z, E_r, H_\vartheta) \sim \cos(n\vartheta), \quad (H_z, H_r, E_\vartheta) \sim \sin(n\vartheta). \quad (6)$$

Also in the cylindrical coordinate system one can get the Bessel equation for the spatial harmonics $f(r)$ of the longitudinal field components $E_z(r)$ or $H_z(r)$ from Maxwell equations:

$$\frac{d^2 f(r)}{dr^2} + \frac{1}{r} \frac{df(r)}{dr} + (k_{sp}^2 - \frac{n^2}{r^2}) f(r) = 0, \quad k_{sp}^2 = k^2 - k_{zp}^2, \quad (7)$$

with the finite solutions at $r = 0$:

$$f(r) = J_n(k_{sp}r), \quad k_{sp}^2 > 0 \quad \text{or} \quad f(r) = I_n(-ik_{sp}r), \quad k_{sp}^2 < 0, \quad (8)$$

where $J_n(x)$ and $I_n(x)$ are Bessel functions of the first order.

In representation (2) all spatial harmonics have different relative phase velocities β_p :

$$\beta_p = \frac{v_p}{c} = \frac{\omega}{ck_{zp}} = \frac{k}{k_{zp}} = \frac{kd}{\Theta_0 + 2p\pi}. \quad (9)$$

The period length d is normally chosen for the synchronous interaction of the particle, moving with velocity $v = \beta c$, $\beta \leq 1$, with a specified, usually the main spatial harmonic ($p = 0$ in (2)) and

$$\beta = \beta_0 \Rightarrow \beta = \frac{kd}{\Theta_0}, \quad d = \frac{\Theta_0\beta}{k} = \frac{\Theta_0\beta\lambda}{2\pi}, \quad (10)$$

where λ is the operating wavelength. From (10, 9, 2) follows $|\beta_p| < 1$ for all $p \neq 0$, resulting always in $k_{sp}^2 = k^2(1 - \frac{1}{\beta_p^2}) \leq 0$, see (8). The modified Bessel functions $I_n(x)$ describe the radial dependences of the spatial harmonics in the representation of the field components (2).

2.2 Properties of Bessel functions

The general expansion of $I_n(x)$ in a power series in x is:

$$I_n(x) = \left(\frac{x}{2}\right)^n \sum_{j=0}^{\infty} \frac{\left(\frac{x}{2}\right)^{2j}}{j!\Gamma(n+j+1)}, \quad I_n^{(1)}(x) = \frac{dI_n(x)}{dx} = I_{n-1}(x) - \frac{n}{x}I_n(x), \quad (11)$$

where $\Gamma(n+j+1)$ is the Gamma function for integer arguments.

For large arguments $x \gg 1$ the functions $I_n(x)$ rises exponentially with increasing argument

$$I_n(x) \approx \frac{e^x}{\sqrt{2\pi x}}. \quad (12)$$

For the approximate estimation of the field components near the axis ($x = k_{sp}^*r \ll 1$) and for the main spatial harmonic with $\beta_0 \rightarrow 1$ we can obtain from (11):

$$I_n(x) \approx \frac{x^n}{2^n(n-1)!} + \frac{x^{n+2}}{2^{n+2}n!} + \dots, \quad I_0(x) \approx 1 + \frac{x^2}{4} + \dots, \quad I_1(x) \approx \frac{x}{2} + \frac{x^3}{8} + \dots, \quad (13)$$

2.3 Field components of dipole mode

For the longitudinal components E_z and H_z of the dipole mode $n = 1$ representation (2) can be rewritten as:

$$E_z(\vartheta, r, z) = \cos(\vartheta) \sum_{p \rightarrow -\infty}^{p \rightarrow +\infty} e_{zp} I_1(k_{sp}^*r) e^{-ik_{zp}z}, \quad k_{sp}^* = -i\sqrt{k_{sp}^2}, \quad (14)$$

$$Z_0 H_z(\vartheta, r, z) = \sin(\vartheta) \sum_{p \rightarrow -\infty}^{p \rightarrow +\infty} Z_0 h_{zp} I_1(k_{sp}^*r) e^{-ik_{zp}z}.$$

Relations for coefficients and radial dependencies for spatial harmonics in the other field components can be expressed from (5) as:

$$\begin{aligned}
k_{sp}^2(r)e_{rp}(r) &= -ik_{zp}k_{sp}^*I_1^{(1)}(k_{sp}^*r)e_{zp} - \frac{ik}{r}I_1(k_{sp}^*r)Z_0h_{zp}, \\
k_{sp}^2e_{\vartheta p}(r) &= \frac{ik_{zp}}{r}I_1(k_{sp}^*r)e_{zp} + ikk_{sp}^*I_1^{(1)}(k_{sp}^*r)Z_0h_{zp}, \\
k_{sp}^2Z_0h_{rp}(r) &= -\frac{ik}{r}I_1(k_{sp}^*r)e_{zp} - ik_{zp}k_{sp}^*I_1^{(1)}(k_{sp}^*r)Z_0h_{zp}, \\
k_{sp}^2Z_0h_{\vartheta p}(r) &= -ikk_{sp}^*I_1^{(1)}(k_{sp}^*r)e_{zp} - \frac{ik_{zp}}{r}I_1(k_{sp}^*r)Z_0h_{zp}.
\end{aligned} \tag{15}$$

2.4 Basis problem. Hybrid waves HE , HM

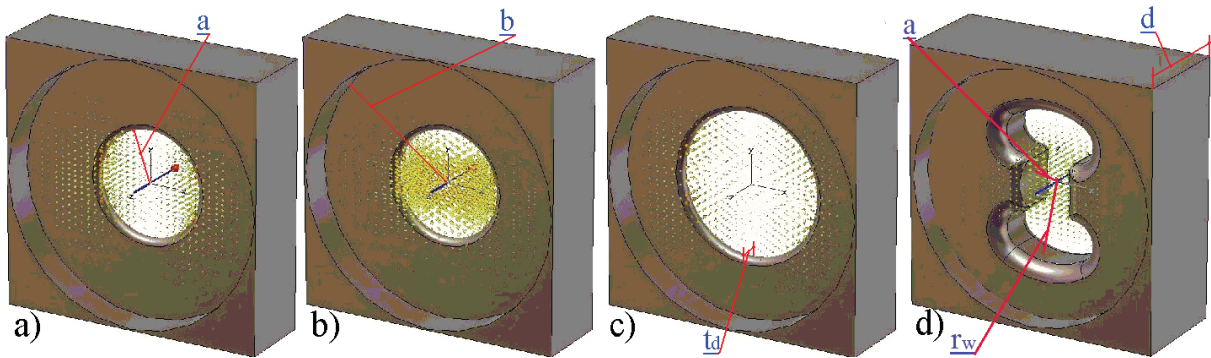


Figure 1: Field distributions for waves with $\Theta_0 = \frac{2\pi}{3}$ with deflecting effect for different structures and modes. a) - with $\frac{a}{\lambda} = 0.23$ at the first DLW passband, $\beta_g < 0$, b) - with $\frac{a}{\lambda} = 0.23$ at the second DLW passband, $\beta_g > 0$, c) - with $\frac{a}{\lambda} = 0.30$ at the first DLW passband, $\beta_g > 0$, d) - with $\frac{a}{\lambda} = 0.067$ at the first passband for a decoupled TE-type structure [4], $\beta_g > 0$.

The representation (5) is the well known description of an arbitrary field in terms of transversal electric TE and transversal magnetic TM waves. In (15) it is detailed for a slow wave system with spatial harmonics. In a mathematical sense it is a basis for a field expansion. This basis works always well, except for one point. For an ultra relativistic particle $\beta = 1$ the synchronous main spatial harmonic $p = 0$ has $k_{z0} = k$, (2,9) and $k_{sp} = 0$, (8) and there is an indefiniteness in the relations (15) between the amplitudes of the field components for the main spatial harmonics.

For $\beta_0 \rightarrow 1$ both TE and TM waves degenerate into a simple plane TEM wave with transversal components only. Attempts for deflecting field description basing only on $TE - TM$ terms are hence not successful.

It is just a methodical problem of the description for the real physical objects - the fields with the effect of deflection. In Fig. 1 the field distributions are shown for different modes and different structures, but all exhibiting effect of deflection. In Fig. 1a, b, c are field distributions in the well known Disk Loaded Waveguide (DLW) shown. The definition of dimensions are: a is the aperture radius, b is the cell radius, t_d is the disk thickness, β_g is the group velocity. A TE-type structure, [4], is shown in Fig. 1d.

Nearly simultaneous investigations in different laboratories, see summarizing papers [5],[6],[7],

resulted in the proposal of another basis for the field representation in cylindrical coordinates. This basis was named as 'hybrid' EH in [5] and [7], $HM - HE$ in [6] and was derived from Herizian vectors as another independent solution of the Helmholtz vector equation.

Such an introduction of additional elements in the basis of waves was not the first one. LE and LM waves were introduced for the $\beta_0 = 1$ case description in rectangular slow wave systems, see the book [9] and references for earlier papers.

Comparison of $TE - TM$ and $HE - HM$ waves is done in [6] and expressions for field components are reproduced here in the Table 1. The $HE_n - HM_n$ waves can be treated as hybrid

Table 1: Field components for the transverse $TE - TM$ and hybrid $HE - HM$ waves, [6].

	TM	TE	HM	HE
$E_r \sim$	$-ik_z \frac{J_n^{(1)}(k_s r)}{k_s^{n-1}}$	$-ik_n \frac{J_n(k_s r)}{k_s^n r}$	$ik k_z \frac{J_{n+1}(k_s r)}{k_s^{n+1}}$	$i(k_z^2 \frac{J_{n+1}(k_s r)}{k_s^{n+1}} + n \frac{J_n(k_s r)}{k_s^n r})$
$E_\vartheta \sim$	$-ik_z n \frac{J_n(k_s r)}{k_s^n r}$	$ik \frac{J_n^{(1)}(k_s r)}{k_s^{n-1}}$	$ik k_z \frac{J_{n+1}(k_s r)}{k_s^{n+1}}$	$i(k^2 \frac{J_{n+1}(k_s r)}{k_s^{n+1}} - n \frac{J_n(k_s r)}{k_s^n r})$
$E_z \sim$	$k_s^2 \frac{J_n(k_s r)}{k_s^n}$	0	$k \frac{J_n(k_s r)}{k_s^n}$	$k_z \frac{J_n(k_s r)}{k_s^n}$
$H_r \sim$	$-ik_n \frac{J_n(k_s r)}{k_s^n r}$	$-ik_z \frac{J_n^{(1)}(k_s r)}{k_s^{n-1}}$	$-i(k_z^2 \frac{J_{n+1}(k_s r)}{k_s^{n+1}} + n \frac{J_n(k_s r)}{k_s^n r})$	$-ik k_z \frac{J_{n+1}(k_s r)}{k_s^{n+1}}$
$H_\vartheta \sim$	$-ik \frac{J_n^{(1)}(k_s r)}{k_s^{n-1}}$	$-ik_z n \frac{J_n(k_s r)}{k_s^n r}$	$i(k^2 \frac{J_{n+1}(k_s r)}{k_s^{n+1}} - n \frac{J_n(k_s r)}{k_s^n r})$	$ik k_z \frac{J_{n+1}(k_s r)}{k_s^{n+1}}$
$H_z \sim$	0	$k_s^2 \frac{J_n(k_s r)}{k_s^n}$	$-k_z \frac{J_n(k_s r)}{k_s^n}$	$-k \frac{J_n(k_s r)}{k_s^n}$

wave with simultaneously exists of all six field components. The longitudinal components E_z and H_z are non vanishing for $k_{sp} = 0$, but are not independent too. For more details of $HE_n - HM_n$ properties see [6] and [5].

As one can see from the Table 1, taking into account the behavior of the Bessel functions(13), for a dipole mode $n = 1$ at the DS axis $r = 0$ an HE_1 wave has non zero transversal components of the electric field E_r, E_ϑ and simultaneously $H_r = H_\vartheta = 0$ at $r = 0$. Non zero transverse components of the magnetic field H_r, H_ϑ at $r = 0$ are represented by an HM_1 wave only. To describe in a real DS the field with simultaneous non zero transverse electric and magnetic components at the axis, we need the linear combination

$$\vec{E} = A\vec{E}_{HE} + B\vec{E}_{HM}, \quad \vec{H} = A\vec{H}_{HE} + B\vec{H}_{HM}, \quad (16)$$

where the coefficients A, B can be defined from the transverse field components E_r, E_x and H_ϑ, H_y distributions at the DS axis.

2.5 Supporting structure

The hybrid waves $HE_n - HM_n$ can not exist without a supporting structure. Differing from $TE_n - TM_n$ waves, hybrid waves can not exist even in a smooth cylindrical waveguide. In a practical sense $HE_n - HM_n$ waves are the tool for deflecting effect description and analysis for the main spatial harmonic in the beam aperture, where the usual $TE_n - TM_n$ basis doesn't work for $\beta_0 = 1$. A preference to describe higher spatial harmonics in terms of $HE_n - HM_n$ is however not evident. It can be done, using the expressions for the field components in the Table 1 and (16), but for all harmonics with $p \neq 0$ the more conventional $TE_n - TM_n$ basis works well.

The complete description of DS parameters in terms of $HE - HM$ waves appears not possible, at least it is not effective. By using the modern software for the numerical simulation of field distributions and frequency calculations, we can estimate all required RF parameters and extract amplitudes of synchronous HE and HM harmonics in the field from the simulated field distribution, basing on (16).

For the DLW structure the solution was obtained in closed form for a small pitch approximation $d \ll \lambda, \frac{t_d}{d} \ll 1, \beta = 1$ in the first passband of dipole modes. From the approximated boundary conditions at $r = a$ both estimation for frequency and for field components (for $r < a$) were obtained [5]:

$$\begin{aligned} E_z(r, \vartheta) &= \frac{E_0}{2}(kr)\cos(\vartheta), & Z_0 H_z(r, \vartheta) &= -\frac{E_0}{2}(kr)\sin(\vartheta), \\ E_r(r, \vartheta) &= i\frac{E_0}{8}(k^2 a^2 + k^2 r^2)\cos(\vartheta), & Z_0 H_r(r, \vartheta) &= i\frac{E_0}{8}(k^2 a^2 - k^2 r^2 - 4)\sin(\vartheta), \\ E_\vartheta(r, \vartheta) &= -i\frac{E_0}{8}(k^2 a^2 - k^2 r^2)\sin(\vartheta), & Z_0 H_\vartheta(r, \vartheta) &= i\frac{E_0}{8}(k^2 a^2 + k^2 r^2 - 4)\cos(\vartheta), \end{aligned} \quad (17)$$

This result is widely used a long time in many papers, see, for example [10], and leads to some important conclusions.

The total flux of traveling RF power P_{tr}^{tot} in a periodical structures is due to the main space harmonic. Using expressions (17), we obtain:

$$P_{tr}^{tot} = \frac{\Re}{2} \int_S ([\vec{E}, \vec{H}^*], \vec{i}_z) dS = \frac{\pi k^2 a^4}{32 Z_0} \left(\frac{k^2 a^2}{3} - 1 \right), \quad (18)$$

For the small aperture radius $ka < \sqrt{3}$ the total power flux $P_{tr}^{tot} < 0, \beta_g < 0$ and DLW in the first dipole passband is a backward wave TW structure. For $ka > \sqrt{3}$ the group velocity is positive and β_g increases with further rise of a . The point $ka = \sqrt{3}, \beta_g = 0$ is known as the inversion point, where β_g changes the sign.

The small pitch approximation is suitable for the description of a DLW operation in Traveling Wave (TW) mode with very low phase advance $\Theta_0 \ll \pi$. For TW mode with $\Theta_0 \geq \pi/2$ or Standing Wave (SW) operation $\Theta_0 = \pi$ the assumption $d \ll \lambda$ is not valid and (17), (18) are just indications.

Considering the DLW deflecting field as the combination of HE_1 and HM_1 waves, from (16), (17) we can define the ratio for the small pitch approximation as

$$\frac{B}{A} = \left(\frac{Z_0 H_\vartheta}{E_r} \right)_{r=0} = \frac{k^2 a^2 - 4}{k^2 a^2}. \quad (19)$$

3 Deflecting field representation and analysis

The Lorenz force acting onto a particle, moving along the z axis with velocity $v = \beta c$ is:

$$\vec{F}_L = e(\vec{E} + [\vec{v}, \vec{B}]) = e(\vec{i}_r(E_r - \beta Z_0 H_\vartheta) + \vec{i}_\vartheta(E_\vartheta + \beta Z_0 H_r) + \vec{i}_z E_z). \quad (20)$$

where e is the electron charge and $\vec{i}_r, \vec{i}_\vartheta, \vec{i}_z$ are unit vectors. The deflecting force F_d and an equivalent deflecting field E_d can be defined through the transverse components of the Lorenz force:

$$\vec{F}_d = e\vec{E}_d = e(\vec{i}_r(E_r - \beta Z_0 H_\vartheta) + \vec{i}_\vartheta(E_\vartheta + \beta Z_0 H_r)). \quad (21)$$

The deflecting field E_d is the linear combination of the original field components. Regardless to a field description in terms of $TM - TE$ or $HM - HE$ waves, each field component can be represented as the sum over spatial harmonics, because (2) is the sequence of the structure periodicity. From linearity, E_d components also can be represented as

$$E_{dr,d\vartheta}(\vartheta, r, z) = \sum_{p \rightarrow -\infty}^{p \rightarrow +\infty} a_{p,dr,d\vartheta}(\vartheta, r) e^{-ik_{zp}z}, \quad (22)$$

where the amplitudes $a_{p,dr,d\vartheta}(\vartheta, r)$ can be obtained, by using (21), from the corresponding amplitudes in the expansions of field components.

In the cylindrical coordinate system the deflecting field amplitude \vec{E}_d can be defined, at least for the main harmonic $p = 0$, [6], from the longitudinal components only, [5]:

$$\vec{F}_d = \frac{e}{k_{z0}} \left(\frac{1 - \beta\beta_0}{1 - \beta_0^2} \nabla_t E_z + \frac{\beta - \beta_0}{1 - \beta_0^2} Z_0 [\vec{i}_z, \nabla_t H_z] \right), \quad \nabla_t = \vec{i}_r \frac{\partial}{\partial r} + \vec{i}_\vartheta \frac{1}{r} \frac{\partial}{\partial \vartheta}, \quad (23)$$

This general expression is valid also for a non synchronous interaction $\beta \neq \beta_0$. For synchronous particle motion $\beta = \beta_0$ relation (23) simplifies as:

$$\vec{F}_d = \frac{e}{k_{z0}} \nabla_t E_z, \quad (24)$$

For ultra relativistic particles ($\beta = 1$) the statement (24) was derived by Panofsky and Wenzel, [8], regardless of a classification of the waves as $TM - TE$ or $HM - HE$.

3.1 Synchronous spatial harmonic

In the analysis of the main spatial harmonic $p = 0$ we have to distinguish two cases - $\beta_0 = 1$ and $\beta_0 < 1$.

For ultra relativistic particles $\beta = \beta_0 = 1$. In this case $k_{z0} = k$ in (2) and $k_{s0}^2 = 0$ in (7) - the Bessel equation degenerates into the Laplace equation for E_z . As one can see from Table 1, HE and HM waves are constructed to have non vanishing E_z and H_z components for $k_{s0}^2 \rightarrow 0$. Expressions for HE and HM field components in the case $\beta_0 = 1, k_{s0}^2 = 0$ also are considered in [6] and reproduced here in the Table 2. By using (24) and $E_z = \frac{E_0 k r}{2}$ for a dipole mode according to Table 2, one can directly get:

$$\vec{F}_d = \frac{eE_0}{2} (\vec{i}_r \cos(\vartheta) - \vec{i}_\vartheta \sin(\vartheta)) = \frac{eE_0}{2} \vec{i}_x. \quad (25)$$

For $\beta_0 = 1$ the deflecting force from the synchronous harmonic, both for HE_1 and HM_1 waves, is constant, both in value and in direction, in all points inside the DS aperture. Due to the

Table 2: Field components for hybrid $HE - HM$ waves with $\beta_0 = 1$, [6].

	HM	HE	ϑ
$E_r \sim$	$i \frac{k^2 r^{n+1}}{2^{n+1}(n+1)!}$	$i \left(\frac{k^2 r^{n+1}}{2^{n+1}(n+1)!} + \frac{r^{n-1}}{2^n(n-1)!} \right)$	$\cos(n\vartheta)$
$E_\vartheta \sim$	$i \frac{k^2 r^{n+1}}{2^{n+1}(n+1)!}$	$i \left(\frac{k^2 r^{n+1}}{2^{n+1}(n+1)!} - \frac{r^{n-1}}{2^n(n-1)!} \right)$	$\sin(n\vartheta)$
$E_z \sim$	$\frac{kr^n}{2^n n!}$	$\frac{kr^n}{2^n n!}$	$\cos(n\vartheta)$
$H_r \sim$	$-i \left(\frac{k^2 r^{n+1}}{2^{n+1}(n+1)!} + \frac{r^{n-1}}{2^n(n-1)!} \right)$	$-i \frac{k^2 r^{n+1}}{2^{n+1}(n+1)!}$	$\sin(n\vartheta)$
$H_\vartheta \sim$	$i \left(\frac{k^2 r^{n+1}}{2^{n+1}(n+1)!} - \frac{r^{n-1}}{2^n(n-1)!} \right)$	$i \frac{k^2 r^{n+1}}{2^{n+1}(n+1)!}$	$\cos(n\vartheta)$
$H_z \sim$	$-\frac{kr^n}{2^n n!}$	$-\frac{kr^n}{2^n n!}$	$\sin(n\vartheta)$

linearity in (24), this statement is also valid for the total field (16). The deflecting force from the synchronous harmonic is free from aberrations.

For the lower phase velocity, $\beta_0 < 1$, the longitudinal component $E_z \sim k \frac{J_1(k_{s0}r)}{k_{s0}}$ for the HM_1 wave and $E_z \sim k_{z0} \frac{J_1(k_{s0}r)}{k_{s0}}$ for the HE_1 wave, see Table 1. Considering the combination $A \cdot HE_1 + B \cdot HM_1$, applying (24) and taking into account $k_{s0}^2 < 0$, we get:

$$\vec{F}_d = \frac{e(Ak_{z0} + Bk)k_{s0}^*}{k_{z0}k_{s0}} (\vec{i}_r I_1^1(k_{s0}^*r) \cos(\vartheta) - \vec{i}_\vartheta \frac{I_1(k_{s0}^*r)}{k_{s0}^*r} \sin(\vartheta)), \quad (26)$$

Using (11) and the approximated expansion (13), in cylindrical coordinates we have:

$$\vec{F}_d \approx \frac{e(Ak_{z0} + Bk)k_{s0}^*}{2k_{z0}k_{s0}} (\vec{i}_r (1 + \frac{(k_{s0}^*r)^2}{4}) \cos(\vartheta) - \vec{i}_\vartheta (1 + \frac{(k_{s0}^*r)^2}{4}) \sin(\vartheta)), \quad (27)$$

We see in the deflecting force non linear additions $\sim (k_{s0}^*r)^2$. Transferring (27) into Cartesian coordinates, we have:

$$\vec{F}_d \approx \vec{i}_x F_x = \vec{i}_x \frac{e(Ak_{z0} + Bk)}{2k_{z0}} \left(1 + \frac{(k_{s0}^*x)^2 + (k_{s0}^*y)^2}{4} \right), \quad F_y \approx 0, \quad (28)$$

The conclusion $F_y \approx 0$ in (28) is due to the expansion limitation in (13) for each Bessel function with two first terms and with additional higher terms $F_y \sim (k_{s0}^*)^4(x^3y + xy^3)$.

For not relativistic case the deflecting force is not free from aberrations - there are non linear additions even in the force from the synchronous harmonic. These inevitable additions are proportional to the constant term in the force and vanish as $\frac{(1-\beta^2)}{\beta^2} = \frac{1}{\gamma^2\beta^2}$ for $\beta \rightarrow 1$, where γ

is the Lorenz factor. The non linear additions in deflecting field x component are always even functions with respect to the planes $x = 0, y = 0$ while the y field component are odd functions. Based on the conclusions (25) and (28) that the deflecting force is directed in the x direction, for simplification of the further analysis of numerical results for different DS's, we will assume equivalent deflecting field at the axis as:

$$E_d = E_x - Z_0\beta H_y, \quad (29)$$

neglecting a possible y component. Transversal y component in the deflecting field can be due to non linear additions only. Moreover, in conversion from cylindrical to Cartesian coordinate systems at the DS axis $r = 0$ for $\vartheta = 0, E_r = E_x, H_\vartheta = H_y$.

From (29) we can define coefficients A, B in the total field representation, because $E_x = AE_x(HE_1)$ from the HE_1 component and $H_y = H_y(HM_1)$ from the HM_1 component in (16).

3.2 Higher spatial harmonics for dipole mode

The higher spatial harmonics $p \neq 0$ in the E_d representation (22) always have a low phase velocity $|\beta_p| < 1$ and $|k_{sp}| \sim |k_{zp}| > k$. Relation (24) for higher harmonics is not proven in [6] and we will use general approach. For transformation reduction, let us consider for beginning spatial harmonics in HE_1 wave only. According to Table 1, the p -th spatial harmonic in the E_z component is:

$$e_{zp}(r) \sim k_{zp} \frac{J_1(k_{sp}r)}{k_{sp}}, \quad \text{or} \quad e_{zp}(r) = C_p I_1(k_{sp}^* r), \quad C_p = const_1 \cdot \frac{k_{zp}}{k_{sp}}. \quad (30)$$

Because E_z and H_z components are not independent in hybrid waves, the respective harmonic in the H_z representation is:

$$h_{zp}(r) = D_p I_1(k_{sp}^* r), \quad D_p = -\frac{C_p k}{k_{zp}}. \quad (31)$$

To define the amplitudes of the spatial harmonics in the transverse field components, we use relations (15), which are a direct consequence of the Maxwell equations. Following (21), the amplitudes of p -th spatial harmonics in the E_d components, assuming $\beta = 1$, are:

$$\begin{aligned} e_{drp}(r) &= e_{rp}(r) - Z_0 h_{\vartheta p}(r) \approx \frac{i(k_{zp} - k)}{2k_{sp}^*} (C_p - D_p) \left(1 + \frac{(k_{sp}^* r)^2}{4}\right) e_{zp}, \\ e_{d\vartheta p}(r) &= e_{\vartheta p}(r) + Z_0 h_{rp}(r) \approx \frac{-i(k_{zp} - k)}{2k_{sp}^*} (C_p - D_p) \left(1 + \frac{(k_{sp}^* r)^2}{4}\right) e_{zp}. \end{aligned} \quad (32)$$

where the approximated expansion (13) is applied. From (33) we get in Cartesian coordinates for the spatial harmonic in the deflecting field due to the HE_1 wave:

$$e_{dxp}(x, y) \approx \frac{i(k_{zp} - k)}{2k_{sp}^*} (C_p - D_p) \left(1 + \frac{(k_{sp}^* x)^2 + (k_{sp}^* y)^2}{4}\right) e_{zp}, \quad e_{dyp}(x, y) \approx 0. \quad (33)$$

A similar expression, but assuming $C_p = const_2 \cdot \frac{k}{k_{sp}}, D_p = -\frac{C_p k_{zp}}{k}$ can be obtained for the spatial harmonic in the deflecting field due to the HM_1 wave.

Considering the deflecting field as combination $A \cdot HE_1 + B \cdot HM_1$, (16), and taking into account

the relations between coefficients C_p and D_p both for the HE_1 and HM_1 waves, for the p -th harmonic in the total deflecting field we get:

$$e_{d_{xp}}(x, y) \approx \frac{ik_{sp}}{2} \left(1 + \frac{(k_{sp}^* x)^2 + (k_{sp}^* y)^2}{4}\right) (A + B) e_{zp}, \quad e_{d_{yp}}(x, y) \approx 0. \quad (34)$$

Here the spatial harmonic e_{zp} for the total E_z component is used. In the derivation of (33) the transformations are the same for the HE_1 and the HM_1 component and $C_p - D_p = \frac{k_{zp} + k}{k_{sp}}$ for both waves.

The relation (34) indicates the possibility that for $A \approx -B$ the amplitude of the p -th spatial harmonic $e_{d_{xp}}(x, y)$ in the deflecting field E_d reduces regardless of the amplitude of the p -th harmonic in the distributions of the original field component e_{zp} .

As one can see, comparing the expressions for the synchronous harmonic $p = 0$ for $\beta < 1$ (28) and for $p \neq 0$, (34), it looks very similar. But there is a big difference. The higher spatial harmonics do not vanish, even for $\beta = 1$. It have a field modulation in the z direction, reflected in (34) by the first multiplier k_{sp} , for a synchronous particle. The constant (with respect x, y) term in the transverse direction in $e_{d_{xp}}$ is modulated in the z direction. As one can estimate from (2), (7), for $|p| > 1$, $|k_{sp}| \sim \frac{2\pi p}{d} \gg k$. Non linear additions in $e_{d_{xp}}$ rise fast with r , as $\sim \left(\frac{2\pi p r}{d}\right)^2$.

The higher spatial harmonics are the main source of non linear additions in the deflecting field distribution.

3.3 Multipole additions

A complete rotational symmetry is not allowed for operating a DS. In this case two waves with deflection in x and in y directions are degenerated in frequency, resulting in not predictable direction of the actual deflection. To cancel the degeneration, in a DLW special holes in the disks are used, which deteriorate the axial symmetry. Also there are DS's, see for example Fig. 1d, which originally have no axial symmetry.

But to support the deflecting mode with $n = 1$, the DS geometry should be symmetric. The deflection in x direction corresponds to zero normal magnetic field at the plane $x = 0$, $H_{norm} = 0$. And the deflecting mode satisfies the boundary condition of zero tangential electric field $E_\tau = 0$ at the plane $y = 0$, $E_\tau = 0$. But these boundary conditions simultaneously satisfy also waves with $n = 3, 5, 7, 9, \dots$

In the field distribution of a real DS, especially with essential deterioration of the rotational symmetry, similar to the DS shown in Fig. 1a, always such higher multipole components $n = 3, 5, 7, \dots$ with a dependence on the azimuth as (6) are present. Similar to spatial harmonics in the deflecting mode, the multipole field components in the beam aperture are required to satisfy the boundary conditions at $r = a$ and decay towards the beam axis. These components should be presented in (2) with additional summations over n . But we can consider the properties of these components independently, due to the linearity of the Maxwell equations.

Let us consider the deflecting field from the first multipole component - the synchronous sextupole wave $n = 3$ for $\beta = 1$. Taking the distribution of the E_z component from Table 2 and using (24) we find:

$$E_z = A_0 \frac{kr^3}{48} \cos(3\vartheta), \quad \vec{F}_d = \frac{eA_0}{16} r^2 (\vec{i}_r \cos(3\vartheta) - \vec{i}_\vartheta \sin(3\vartheta)) \quad (35)$$

Transferring to Cartesian coordinates,

$$\vec{F}_d = \frac{eA_0}{16}(\vec{i}_x(x^2 - y^2) + \vec{i}_y 2xy). \quad (36)$$

The transverse force from multipole components even for the synchronous harmonics has only non linear terms. They are non vanishing synchronous additions. The amplitudes of multipole additions depend on the DS geometry and should be minimized, as far as possible, during the DS shape development.

Similar to the dipole mode, we can consider the spatial harmonics for multipole waves. Always it will be just nonlinear additions, starting with higher power than x^2, y^2 . The higher spatial harmonics in the multipole component decay faster toward the beam axis and are hence not so dangerous for the field quality as synchronous multipole waves.

3.4 Bunch deflection and bunch rotation

Let us consider the difference between bunch deflection and bunch rotation for a TW operating mode.

The force from the field component $E_j(\vartheta, r, z)$ in (1) on the particle, moving with velocity βc , is:

$$\frac{F_j(\vartheta, r, z)}{e} = \Re E_j(\widehat{\vartheta}, r, z) e^{i(\psi_j(\vartheta, r, z) + k_{z0}z + \phi)}, \quad \omega t = \frac{\omega z}{\beta c} = k_{z0}z, \quad (37)$$

where ϕ is the initial phase shift between the particle and the wave.

For bunch deflection $\phi = 0$ for the central particle and, using (22) for the deflecting field, from (37) it follows:

$$\frac{F_{dr, d\vartheta}(\vartheta, r, z)}{e} = a_{d0, dr, d\vartheta}(\vartheta, r) + \sum_{p=1} a_{dp, dr, d\vartheta}(\vartheta, r) \cos\left(\frac{2p\pi z}{d}\right). \quad (38)$$

The particles get a permanent deflection from the synchronous interaction with the main harmonic $p = 0$ and the bunch oscillates as a whole with respect of the deflection direction. Usually the main spatial harmonic dominates in the field expansion and the effect of higher spatial harmonics can be acceptable for bunch deflection the bunch oscillation is in the background of the dominating deflection. In bunch deflection mode exists an analogy with the particle acceleration due to a longitudinal field - there is a permanent acceleration from the synchronous harmonic and oscillations with respect to the synchronous motion due to the interaction with higher spatial harmonics.

For the general description of an accelerating field in accelerating structures the transit time factor T_z is used and we can define in an equivalent way the transit time factor T_d for the deflecting field at the DS axis:

$$T_z = \frac{|\int_{-\frac{d}{2}}^{\frac{d}{2}} E_z(z) e^{ik_{z0}z} dz|}{\int_{-\frac{d}{2}}^{\frac{d}{2}} \widehat{E}_z(z) dz}, \quad T_d = \frac{|\int_{-\frac{d}{2}}^{\frac{d}{2}} E_d(z) e^{ik_{z0}z} dz|}{\int_{-\frac{d}{2}}^{\frac{d}{2}} \widehat{E}_d(z) dz} \quad (39)$$

For bunch rotation $\phi = \frac{\pi}{2}$ and, similar to (38),

$$\frac{F_{dr, d\vartheta}(\vartheta, r, z)}{e} = \sum_{p=1} a_{dp, dr, d\vartheta}(\vartheta, r) \sin\left(\frac{2p\pi z}{d}\right). \quad (40)$$

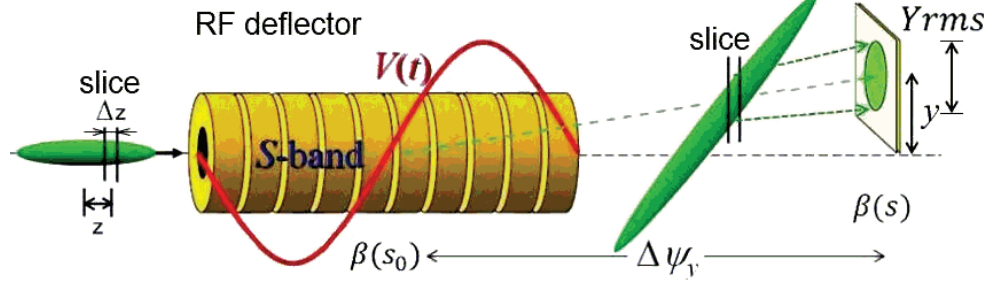


Figure 2: Illustration of the bunch rotation for measurements of longitudinal distributions, [11].

Schematically a bunch rotation is illustrated in Fig. 2, see [11] for more explanations about measurements of bunch parameters. During bunch rotation the central bunch particle doesn't see the main spatial harmonic and moves along the DS axis. But upstream and downstream particles will receive a synchronous deflection in opposite directions - the bunch rotates. Together with the synchronous rotation, the bunch oscillates as a whole with respect to the DS axis due to the higher spatial harmonics in (40).

In structures with planes of mirror symmetry the effective deflecting field in (38) is an even function on z with respect to the mirror planes and the residual field in (40) is an odd function.

3.5 Criterion for higher harmonics estimation in periodical structures

To compare different DS realizations with respect to the relative level of higher harmonics in the field distributions, we need a criterion for this comparison.

Let us consider the phase dependence $\psi_j(\vartheta, r, z)$ in (1). Subtracting the synchronous spatial harmonics from the phase distribution, from (2) we get:

$$E_j(\vartheta, r, z) = E_j(\widehat{\vartheta}, r, z) e^{i\psi_j(\vartheta, r, z) + k_{z0}z} = \sum_{p \rightarrow -\infty}^{p \rightarrow +\infty} a_{jp}(\vartheta, r) e^{-i\frac{2p\pi z}{d}}, \quad (41)$$

or

$$\begin{aligned} \Re E_j(\widehat{\vartheta}, r, z) e^{i\psi_j(\vartheta, r, z) + k_{z0}z} &= \sum_{p=0} a_{jp}(\vartheta, r) \cos\left(\frac{2p\pi z}{d}\right), \\ \Im E_j(\widehat{\vartheta}, r, z) e^{i\psi_j(\vartheta, r, z) + k_{z0}z} &= -\sum_{p=1} a_{jp}(\vartheta, r) \sin\left(\frac{2p\pi z}{d}\right). \end{aligned} \quad (42)$$

In (42) we find a simple expansion in a Fourier set, where

$$a_{jp}(\vartheta, r) = \frac{1}{d} \int_{-\frac{d}{2}}^{\frac{d}{2}} E_j(\vartheta, r, z) \sin(\psi_j(\vartheta, r, z) + k_{z0}z) \sin\left(\frac{2p\pi z}{d}\right) dz. \quad (43)$$

Spatial harmonics are essential at the aperture radius $r = a$ and we can assume $a_{jp}(\vartheta, a) \sim a_{0p}(\vartheta, a)$. As one can see from (14) and (15), the distributions for harmonics are described with

combinations of Bessel functions. According to (12), the higher harmonics $|p| \gg 1$ attenuate to the axis as:

$$a_{jp}(0) \sim a_{jp}(a) \cdot \exp\left(-\frac{4\pi^2|p|}{\beta\Theta_0} \cdot \frac{a}{\lambda}\right). \quad (44)$$

At the beam axis $r = 0$ just the lower harmonics $p = \pm 1, \pm 2, \pm 3$ are really essential.

For an 'in total' estimation of the harmonic content we will consider the deviation of the total phase distribution $\psi_j(\vartheta, r, z)$ at the axis from the phase of the synchronous harmonic $\delta\psi_j(z)$ and use the parameter Ψ_j

$$\delta\psi_j(z) = \psi_j(z) + \frac{\Theta_0 z}{d}, \quad \Psi_j = \max(|\delta\psi_j(z)|), \quad 0 \leq z \leq d, r = 0. \quad (45)$$

From symmetry properties $\delta\psi_j(z)$ is always an odd function with respect to the mirror symmetry planes and we can use only half of period length in (45). For the cases of our interest $|a_{jp}| \ll |a_{0p}|$ it is $\sim \sin(\frac{2\pi iz}{d})$ function with small deviations due to the second and the third harmonics. In this case the usage of Ψ_j instead of $\delta\psi_j(z)$ in (43) will lead to an upper estimation of $a_{jp}(0)$ and smaller values of Ψ_j correspond to smaller values of $a_{jp}(0)$.

The slow wave system with perfectly linear phase dependence $\psi_j(\vartheta, r, z)$ is not possible, because it means $\delta\psi_j(z) = 0$ and, from (43), $a_{jp} = 0, |p| \neq 0$ corresponds to a single wave, which can exist only in a smooth waveguide. But slow wave systems with essentially damped harmonics at the beam axis are possible.

3.6 Panofsky-Wenzel theorem

The relationship

$$\vec{p}_t = -i\left(\frac{ec}{\omega}\right) \int_0^L \nabla_t E_z dz \quad (46)$$

where \vec{p}_t is the transverse particle momentum gain, has been derived in [8] regardless of the field classification, but with an important assumption the particle velocity is large enough to allow the particle direction to remain essentially unchanged by the transverse force. It is the case $\beta = 1$. For lower electron energy this statement is a framework.

As one can see comparing (24) and (46), both formulations lead to similar value of the deflecting force. But in (46) the total value of the E_z component, without specification of the synchronous space harmonic, is used.

From the Maxwell equation $rot\vec{E} = -\frac{\partial\vec{B}}{\partial t}$ we find directly:

$$\frac{\partial E_z}{\partial r} = \frac{\partial E_r}{\partial z} + ikZ_0 H_\vartheta \quad \text{or} \quad \frac{\partial E_z}{\partial x} = \frac{\partial E_x}{\partial z} + ikZ_0 H_y. \quad (47)$$

We can expand each component either into a Fourier series over space harmonics, (2) (discrete k_{zp} spectrum for periodical structures) or provide a Fourier transform - continuous k_{zp} spectrum for single cavity. The interaction with a particle, traveling along z with unchanged velocity, is described by $e^{ik_{z0}z}$ and will select only the synchronous component. With the inverse transformation, we obtain:

$$\frac{\partial e_{z0}(r)}{\partial r} = -ik_{z0}(e_{r0}(r) + \beta_0 Z_0 h_{\vartheta 0}(r)) = -ik_{z0}e_{d0}(r), \quad (48)$$

where e_{d0} is the amplitude of the synchronous harmonic of the equivalent deflecting field, see (21).

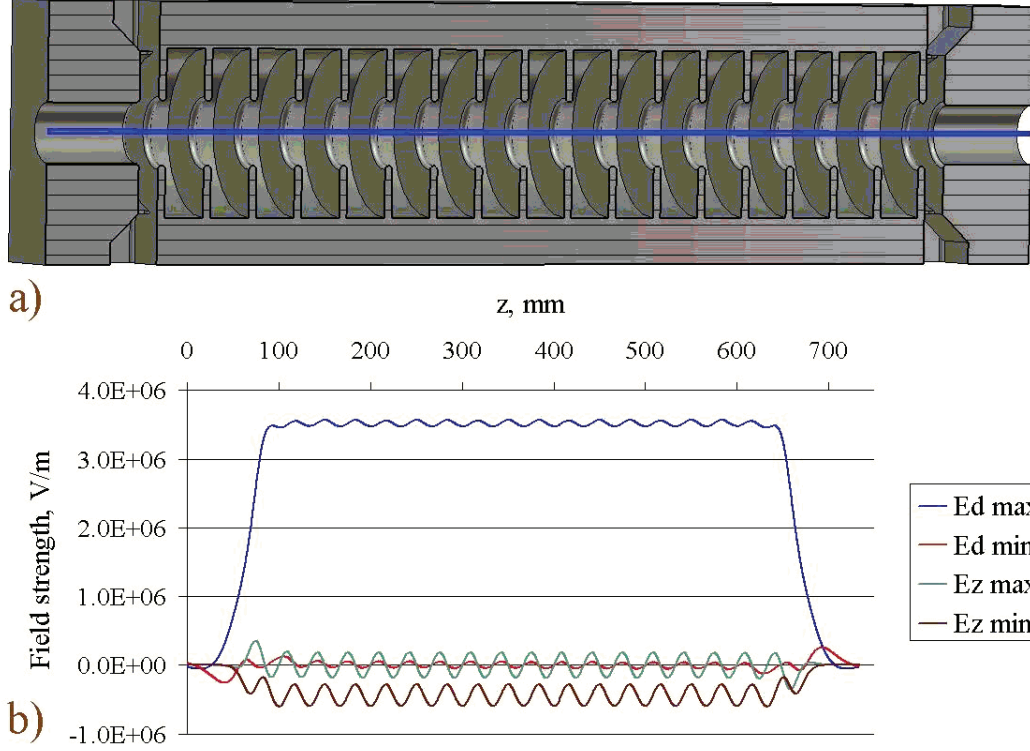


Figure 3: A TW DLW structure (a) with $\Theta_0 = \frac{2\pi}{3}$ and field distributions for E_d at the axis, $\phi_0 = 0$ (dark blue) and $\phi_0 = \frac{\pi}{2}$ (red), and E_z distribution along the line $x = 2mm$ also for $\phi_0 = 0$ (blue) and $\phi_0 = \frac{\pi}{2}$ (brown).

As one can see from expressions for $HM - HE$ wave components in the Table 2, for a dipole mode $E_z(r) \sim kr, \Rightarrow \frac{\partial E_z(r)}{\partial r} \sim k$. Instead of the representation via the total E_z component, the coupling of longitudinal and transverse motion is generated through the synchronous harmonics. This theorem provides an important indication the longitudinal and transverse forces are shifted in phase at $\frac{\pi}{2}$.

In Fig. 3a a TW deflecting structure with operating phase advance $\Theta_0 = \frac{2\pi}{3}$ is shown. This structure is the well known LOLA IV option, [13], scaled to an operating frequency of $3000MHz$ and differing in the design of the RF couplers. In Fig. 3b the distributions of E_d and E_z are shown for an operation in bunch deflection ($\phi_0 = 0$) and bunch rotation mode ($\phi_0 = \frac{\pi}{2}$). The plots in Fig. 3b illustrate - for bunch deflection E_d is maximal, but the average E_z is zero and there are only oscillations due to $E_z(z)$, similar to (40). The bunch deflection is not accompanied by an average change in the longitudinal momentum. For bunch rotation E_d is zero on average, according (40), while E_z is on average not zero, similar to (38). The bunch rotation is accompanied by an average change in the longitudinal particle momentum which is proportional to radial particle position.

4 Traveling and standing wave operation

Let us consider some differences due to different operating modes of DS.

4.1 Deflecting field distributions for TW and SW mode

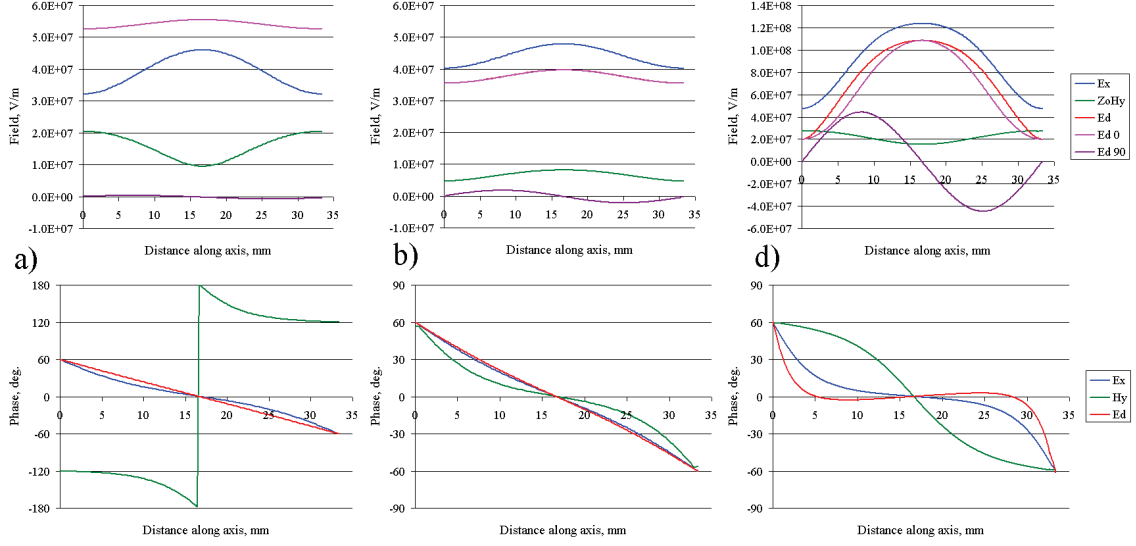


Figure 4: The distributions of amplitudes for E_x , $Z_0 H_y$ and deflecting field E_d , $\phi = 0$ and E_d , $\phi = 90$ (upper row) and distribution of phases for E_x , H_y and E_d (bottom row) for DS's, shown in Fig. 1a, b and d, TW operating mode, $\Theta_0 = \frac{2\pi}{3}$.

For a TW mode each field component has both real and imaginary parts. The amplitudes of all spatial harmonics in (2) are constant over the structure period d . Considering the deflecting field composed as (21) or (29), for the deflecting force, similar to (37), we have at the DS axis:

$$\begin{aligned} \frac{F_d(z)}{e} &= \Re\left(\sum_{p=0} (e_{rp} - Z_0 h_{\vartheta p}) e^{i(k_{zp} + k_{z0}z + \phi)}\right) = (e_{r0} - Z_0 h_{\vartheta 0}) \cos(\phi) + \\ &+ \cos(\phi) \sum_{p=1} (e_{rp} - Z_0 h_{\vartheta p}) \cos\left(\frac{2p\pi z}{d}\right) + \sin(\phi) \sum_{p=1} (e_{rp} - Z_0 h_{\vartheta p}) \sin\left(\frac{2p\pi z}{d}\right). \end{aligned} \quad (49)$$

In Fig. 4 the distribution of the amplitudes for $E_r = E_x$, $Z_0 H_\vartheta = Z_0 H_y$ and the deflecting fields E_d , $\phi = 0$ and E_d , $\phi = \frac{\pi}{2}$ (upper row) and the distribution of the phase for E_x , H_y and E_d (bottom row) for the DS, shown in Fig. 1a, b and d, assuming a TW operating mode with $\Theta_0 = \frac{2\pi}{3}$, are shown. There are some differences in deflecting field distributions due to different phasing and balance of hybrid waves HE_1 and HM_1 in (16), but the common properties are the same:

The interaction with the synchronous harmonic is constant over the period, regardless to the ratio of e_{r0} and $Z_0 h_{\vartheta 0}$ components. Always an initial phase shift $\phi = \frac{\pi}{2}$ between the wave and the central particle of the bunch exists when the central particle doesn't see the synchronous harmonic i.e. the perfect bunch rotation operating mode. Always oscillations of E_d take place due to higher spatial harmonics only.

For TW mode harmonics the attenuation (44) works for all original field components and is especially essential for lower phase advance $\Theta_0 \ll \pi$. Every DS, operating in TW mode with a low phase advance, has a reduced level of spatial harmonics, both for the longitudinal and transverse field components. For the deflecting field E_d , composed from electric and magnetic components of the original field, further reduction of harmonics takes place for opposite phasing

of HE_1 and HM_1 waves, $A \cdot B < 0$ in (16). According to (34), we can expect $|e_{dp}| \ll |e_{zp}|$ for $A \sim -B$.

The criterion for harmonics estimation (45) in TW mode works naturally both for longitudinal and transverse components of the Lorenz force (20). The minimal value of Ψ_d corresponds to a minimal level of spatial harmonics for bunch rotation $\phi = \frac{\pi}{2}$ and, simultaneously, for bunch deflection $\phi = 0$, according to (43).

For SW operation mode the field distribution for $0 < \Theta_0 < \pi$ can be obtained as the sum of the forward wave $E_j(\vartheta, r, z)$, (2), and the backward wave $E_j^*(\vartheta, r, z)$. But for $\Theta_0 = 0, \pi$ the forward and the backward waves are identical, [9]. A specific case of a compensated structures is, see [3], when at the operating frequency two 0 or two π modes from two different passbands, which have a conjugated parity of field distributions with respect to mirror symmetry planes, coincide. There is just one proposal of the compensated DS known, [12], which is not realized in practice.

As for every periodical structure, SW modes for DS with $0 < \Theta_0 < \pi$ are not effective with respect to the RF parameters. There are no references for DS, operating with $\Theta_0 = 0$ or $\Theta_0 = 2\pi$. Considering DS SW operation, we assume in the following $\Theta_0 = \pi$.

For the SW case each field component $E_j(\vartheta, r, z)$ in (1) has only either real or imaginary

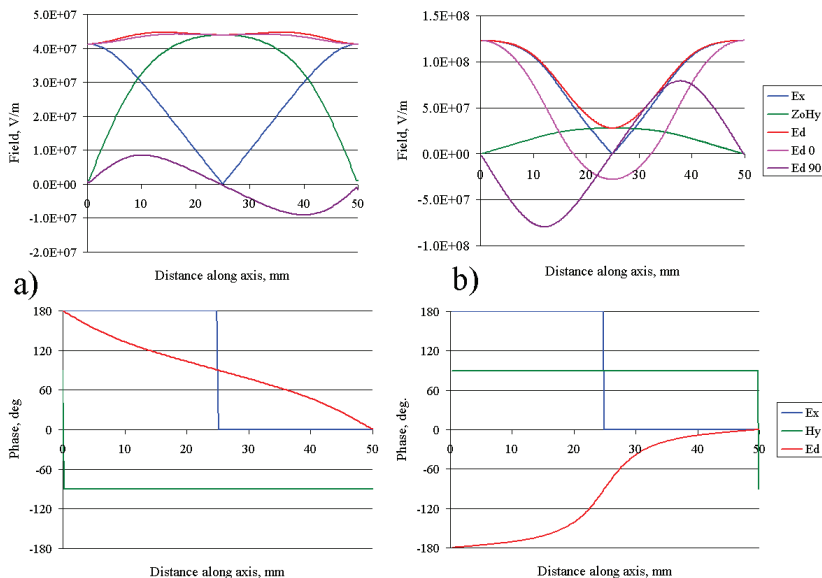


Figure 5: The distributions of amplitudes for E_x , $Z_0 H_y$ and E_d , deflecting field E_d , $\phi = 0$ and E_d , $\phi = 90$ (upper row) and distribution of phase for E_x , H_y and E_d (bottom row) for DLW with $\frac{a}{\lambda} = 0.18$, (a) and for decoupled DS, Fig. 1d, $\frac{a}{\lambda} = 0.07$, $\Theta_0 = \pi$.

part and the phase $\psi_j(\vartheta, r, z)$ is a step-wise function with one step of π over the period. The periodicity in the field distribution, similar to (2) and the linearity in (21) remain.

For each component separately $\Psi_j = \frac{\pi}{2}$ holds, according to (45). The longitudinal component in the Lorenz force (20) is only due to the E_z component and a reduction of harmonics can be obtained only due to attenuation (44), which is not so effective for lower harmonics at $\Theta_0 = \pi$. Typical values of T_z , (39), are $T_z \approx (0.75 \div 0.8)$, $e_{z1} \sim 0.6$. A reduction of aberrations in the longitudinal force component for the SW mode can be achieved only at the expense of an increased aperture radius.

In Fig. 5 the distributions of amplitudes for $E_r = E_x$, $Z_0H_\vartheta = Z_0H_y$ and deflecting fields E_d , $\phi = 0$ and E_d , $\phi = \frac{\pi}{2}$ (upper row) and distributions of phase for E_x , H_y and E_d (bottom row) for DLW $\frac{a}{\lambda} = 0.18$, (a) and for decoupled DS, Fig. 1d, $\frac{a}{\lambda} = 0.07$ are shown for SW operation mode.

Taking into account DS symmetry properties, for deflecting field E_{dr} we can write:

$$E_{dr}(z) = \cos(\omega t + \phi) \cdot \sum_{p=0} e_{rp} \cos\left(\frac{(\pi + 2p\pi)z}{d}\right) - \sin(\omega t + \phi) \cdot \sum_{p=0} Z_0 h_{\vartheta p} \sin\left(\frac{(\pi + 2p\pi)z}{d}\right). \quad (50)$$

Considering just the main harmonics $p = 0$ for the synchronous particle $\omega t = kz = \frac{\pi z}{d}$, we see:

$$\begin{aligned} E_{dr}(z) &= e_{r0} \cos(kz + \phi) \cos(kz) - Z_0 h_{\vartheta 0} \sin(kz + \phi) \sin(kz) = \\ &= \frac{e_{r0} - Z_0 h_{\vartheta 0}}{2} \cdot \cos(\phi) + \frac{e_{r0} + Z_0 h_{\vartheta 0}}{2} \cdot \cos(2kz + \phi) \end{aligned} \quad (51)$$

For any initial phase shift ϕ the central particle sees both a uniform and an oscillating impact of the deflecting field. Even if the main harmonics are free from aberrations, the oscillating part in (51) shifts the particle from the DS axis to regions with higher field nonlinearities from the spatial harmonics. As one can see from (51), the ratio of uniform and oscillating parts depends on the phasing and the balance of the synchronous harmonics e_{r0} and $Z_0 h_{\vartheta 0}$. For opposite phasing $e_{r0} \cdot Z_0 h_{\vartheta 0} < 0$ the amplitude of the uniform deflection $e_{r0} - Z_0 h_{\vartheta 0}$ exceeds the amplitude of the oscillations $e_{r0} + Z_0 h_{\vartheta 0}$. For the case $e_{r0} = -Z_0 h_{\vartheta 0}$, corresponding to $A = -B$ in (16), the central particle moves under action of the synchronous field harmonics without oscillations and the perfect bunch rotation is possible for $\phi = \frac{\pi}{2}$.

Taking into account the spatial harmonics in the E_r and H_ϑ field components, for the deflecting field one can get:

$$\begin{aligned} E_{dr}(z) &= \frac{e_{r0} - Z_0 h_{\vartheta 0}}{2} \cdot \cos(\phi) + \\ &+ \frac{\cos\phi}{2} \cdot \sum_{p=1} (e_{rp-1} + Z_0 h_{\vartheta p-1} + e_{rp} - Z_0 h_{\vartheta p}) \cos\left(\frac{2p\pi z}{d}\right) - \\ &- \frac{\sin\phi}{2} \cdot \sum_{p=1} (e_{rp-1} + Z_0 h_{\vartheta p-1} - e_{rp} + Z_0 h_{\vartheta p}) \sin\left(\frac{2p\pi z}{d}\right). \end{aligned} \quad (52)$$

This is the general case of the force onto the central particle from the force sources, E_r and H_ϑ , which are shifted both in distance along the axis and in time. As one can see the amplitudes of the p -th and $p - 1$ harmonics are coupled in the amplitudes of the oscillations $\sim \sin(\frac{2p\pi z}{d})$, $\sim \cos(\frac{2p\pi z}{d})$. Just for the case $e_{r0} = -Z_0 h_{\vartheta 0}$ oscillations appear due to the higher spatial harmonics only. For equal phasing $e_{r0} \cdot Z_0 h_{\vartheta 0} > 0$ the amplitude of the oscillations can exceed the average value of deflecting field.

We can rewrite (52) as:

$$\begin{aligned} E_{dr}(z) &= \frac{e'_{d0}}{2} \cdot \cos\phi + \frac{\cos\phi}{2} \cdot \sum_{p=1} e_{dp}^e \cos\left(\frac{2p\pi z}{d}\right) - \frac{\sin\phi}{2} \cdot \sum_{p=1} e_{dp}^o \sin\left(\frac{2p\pi z}{d}\right). \\ e'_{d0} &= e_{r0} - Z_0 h_{\vartheta 0}, \quad e_{dp}^e = e_{rp-1} + Z_0 h_{\vartheta p-1} + e_{rp} - Z_0 h_{\vartheta p}, \\ &e_{dp}^o = e_{rp-1} + Z_0 h_{\vartheta p-1} - e_{rp} + Z_0 h_{\vartheta p}. \end{aligned} \quad (53)$$

As one can see from (53), the amplitudes of the even oscillating terms e_{dp}^e differ from the amplitudes of the odd oscillating terms e_{dp}^o for the same p .

The criterion for harmonics estimation (45) in SW mode works formally as for a TW mode. Taking into account the time dependence, for deflecting field we can write:

$$E_{dr}(z)e^{i\omega t} = (E_r(z) - iZ_0H_{\vartheta}(z))e^{i\omega t} \quad \text{or} \quad E_{dr}(z)e^{ikz} = (E_r(z) - iZ_0H_{\vartheta}(z))e^{ikz}. \quad (54)$$

and can consider $E_{dr}(z)e^{ikz}$ as a complex function with real and the imaginary parts, which describes an 'equivalent' traveling wave. In a mathematical sense the parameter $\Psi_d = \max(|\delta\psi_d(z)|)$ reflects the imaginary part of the complex function (54). For the opposite $e_{r0}, h_{\vartheta0}$ phasing $e_{r0} \cdot Z_0h_{\vartheta0} < 0$ the parameter Ψ_d reflects 'in total' the oscillating part in (54), which is described by the odd oscillating terms e_{dp}^o , including both higher spatial harmonics and oscillations due to the not compensated term $e_{r0} + Z_0h_{\vartheta0} \neq 0$ in the main harmonics. Thus the condition $(\Psi_d)_{min}$ corresponds to the most uniform motion of the central particle near the axis during bunch rotation for a SW mode. But the E_d distribution for the bunch deflection condition $(\Psi_d)_{min}$ corresponds due to the e_{dp}^o and e_{dp}^e difference not to the minimal level of oscillating additions. In the distribution $E_d(z), \phi = 0$, obtained for the condition $(\Psi_d)_{min}$ we will always have larger deviations from the average value, than in the distribution $E_d(z), \phi = \frac{\pi}{2}$. For equal $e_{r0}, h_{\vartheta0}$ phasing the parameter Ψ_d is not useful, because the 'equivalent' traveling wave in (54) is the backward wave with respect to the central particle and $(\Psi_d)_{min} = \pi$. But for equal phasing we have both strong oscillations due to the main harmonics, according to (52), and increased amplitudes for higher E_d harmonics, according to (34).

4.2 Phase deviations in deflecting field distribution

Suppose for a TW mode we have at the DS axis a phase deviation $d\psi_d(z)$ in the phase distribution $\psi_d(\vartheta, r, z)$ of the deflecting field due to some reasons. Similar to (37) and (38), the force from the deflecting field for bunch deflection is:

$$\begin{aligned} \frac{F_d(z)}{e} &= \Re(\widehat{E_d}(z)e^{i(\psi(z)+k_{z0}z+d\psi_d(z))}) = \widehat{E_d}(z)\cos(\delta\psi_d(z) + d\psi_d(z)) = \\ &= \cos(d\psi_d(z)) \cdot (e_{d0} + \sum_{p=1} e_{dp}\cos(\frac{2p\pi z}{d})) - \sin(d\psi_d(z)) \cdot \sum_{p=1} e_{dp}\sin(\frac{2p\pi z}{d}). \end{aligned} \quad (55)$$

where (38) and (40) are taken into account. For bunch rotation

$$\begin{aligned} \frac{F_d(z)}{e} &= \Re(\widehat{E_j}(z)e^{i(\psi(z)+k_{z0}z+d\psi_d(z)+\pi/2)}) = \widehat{E_d}(z)\sin(\delta\psi_d(z) + d\psi_d(z)) = \\ &= \sin(d\psi_d(z)) \cdot (e_{d0} + \sum_{p=1} e_{dp}\cos(\frac{2p\pi z}{d})) + \cos(d\psi_d(z)) \cdot \sum_{p=1} e_{dp}\sin(\frac{2p\pi z}{d}). \end{aligned} \quad (56)$$

From (55) and (56) we see a quite different role of the phase deviation $d\psi_d(z)$ for bunch deflection and bunch rotation. For small deviations $|d\psi_d(z)| \ll 1$

$$\cos(d\psi_d(z)) \approx 1 - \frac{(d\psi_d(z))^2}{2}, \quad \sin(d\psi_d(z)) \approx d\psi_d(z). \quad (57)$$

For bunch deflection the phase deviations $d\psi_d(z)$ leads to a second order change in the distribution of the deflecting field (38) and to the generation of small residual field (40). For a bunch rotation mode the phase deviations immediately generate a bunch deflection $\approx e_{d0}d\psi_d(z)$ by the synchronous harmonic. At the plots of $E_d(z), \phi = \pi/2$ arise peaks of E_d and the bunch as

a whole will be deflected from the axis, similar to the oscillations in (51), with the same effect. The bunch will be displaced as a whole from the axis to a region with higher level of nonlinear additions in the field distributions.

We have to distinguish possible reasons of phase deviations. The first reason are possible errors in the cell frequencies. It can be reduced by appropriate RF tuning.

The second reason are violations of the structure periodicity - RF coupler cell, end cell with connected beam pipe and so on. For such elements special attention is required.

The criterion for spatial harmonics estimation, introduced in (45), works well also for the total structure, including cells with violated periodicity. If we see large phase deviation in the RF coupler cell from the phase of the synchronous particle, according to (56) we will have corresponding unwanted peaks in the E_d distribution for bunch rotation. Reduction of the phase deviation $d\psi_d(z)$ simultaneously leads to a reduction of the peaks.

4.3 RF efficiency for TW and SW mode

Both for bunch deflection and bunch rotation we need the value of deflecting voltage V_d for a specified RF power P .

For SW mode all RF power is dissipated in the cavity surface and V_d is directly related to the effective transverse shunt impedance $Z_e^{(SW)}$ per unit length:

$$Z_e^{(SW)} = \frac{|\frac{1}{k} \int_0^L \frac{\partial E_z}{\partial z} e^{ikz_0 z} dz|^2}{P_s L} = \frac{(E_{d0} L)^2}{P_s L}, \quad \beta = 1, \quad (58)$$

where L is the total structure length. This definition of Z_e is based on the Panofsky-Wenzel theorem.

For TW mode the wave propagates along the structure, both providing the required field and attenuating in amplitude due to RF power dissipation in the surface of the structure. The rest of the RF power comes to the RF load at the end of the TW structure. The TW structure parameter, independent with respect to frequency scaling, is the normalized field strength:

$$\frac{E_{d0} \lambda}{\sqrt{P_t}} = \sqrt{\frac{2\pi \lambda Z_e^{(TW)}}{|\beta_g| Q}}, \quad (59)$$

where $Z_e^{(TW)}$ is defined similar to (58), E_{d0} is the field value for the synchronous deflecting harmonic and P_t is the RF power flux. The total deflecting voltage $V_d^{(TW)}$ is:

$$V_d^{(TW)} = \int_0^L E_{d0}^{(i)} e^{-\alpha z} dz = \frac{E_{d0}^{(i)}}{\alpha} (1 - e^{-\alpha L}), \quad (60)$$

where α is the attenuation constant $\alpha = \frac{\pi}{\lambda |\beta_g| Q}$ and $E_{d0}^{(i)}$ is the value of E_{d0} at the beginning of the TW structure.

Assuming the structure is not so long, $\alpha L \ll 1$, and estimating $Z_e^{(SW)} \approx Z_e^{(TW)}$, from (58) - (60) we can estimate the ratio:

$$\frac{V_d^{(TW)}}{V_d^{(SW)}} \approx \sqrt{\frac{2\pi L}{\lambda |\beta_g| Q}}. \quad (61)$$

For structures operated as TW the choice of $|\beta_g|$ is of primary importance, simultaneously defining both positive and negative DS properties - RF efficiency (59) as $\sim (|\beta_g|)^{-\frac{1}{2}}$, wave

attenuation $\alpha \sim (|\beta_g|)^{-1}$, phase distribution sensitivity to cell frequencies deviations $\sim (|\beta_g|)^{-1}$. A typical value of $(|\beta_g|) \sim 10^{-2}$ is usually accepted as a compromise. For S -band applications, $\lambda = 0.1m, Q \sim 10^4$ one can conclude from (61) - for structure length $L < 1$ m SW operating regime is more effective to obtain required value of V_d .

5 Parameters of the DLW structure

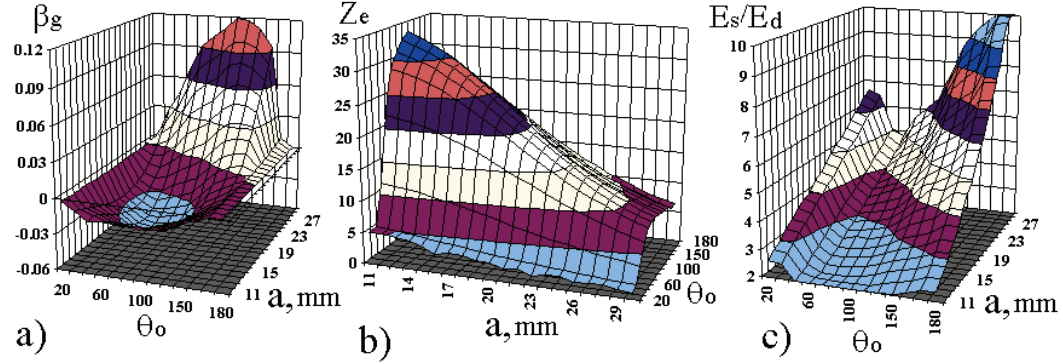


Figure 6: The surfaces $\beta_g(a, \Theta_0)$ (a), $Z_e(a, \Theta_0)$ (b) and $\frac{E_s}{E_d}(a, \Theta_0)$ for a DLW structure, $\frac{td}{\lambda} = 0.054, \lambda = 10cm$.

The study of DLW parameters has been performed in a wide range of operating parameters $\frac{\pi}{9} \leq \Theta_0 \leq \pi$ and for aperture radii a in the range of $0.11 \leq \frac{a}{\lambda} \leq 0.30$, assuming $\lambda = 10cm$. Always the E_z distribution is calculated along the line $x = 2mm$. The results are presented in Fig. 6 and Fig. 7 as two dimensional surfaces to have general view for the DLW properties. In Fig. 6 the surfaces for group velocity $\beta_g(a, \Theta_0)$, Fig. 6a, effective transverse shunt impedance $Z_e(a, \Theta_0)$ and ratio $\frac{E_s}{E_d}(a, \Theta_0)$, where E_s is the maximal electric field at the surface, are plotted. As it is common for slow wave structures, $\beta_g(a, \Theta_0) \rightarrow 0, \Theta_0 \rightarrow 0, \pi$. For each intermediate value of $\Theta_0 \neq 0, \pi$ there is the inversion point, (18), $(\frac{a}{\lambda})_{inv}(\Theta_0)$ corresponding to $\beta_g = 0$. Below this point $(\frac{a}{\lambda}) < (\frac{a}{\lambda})_{inv}$ the group velocity is negative $\beta_g(\frac{a}{\lambda}) < 0$, corresponding to the backward traveling wave. For $(\frac{a}{\lambda}) > (\frac{a}{\lambda})_{inv}$ the group velocity is positive $\beta_g(\frac{a}{\lambda}) > 0$, corresponding to the forward wave.

The surface $Z_e(a, \Theta_0)$ has an upland for $\Theta_0 \approx \frac{\pi}{2}$ and the general trend is that Z_e decreases with increasing a .

The surface of the ratio $\frac{E_s}{E_d}$ has a valley for $\Theta_0 \approx \frac{\pi}{3}$ and the general trend is that $\frac{E_s}{E_d}$ increases with increasing a .

In Fig. 7 the surfaces $\Psi_{zm}(a, \Theta_0)$, Fig. 7a, $T_z(a, \Theta_0)$, Fig. 7b, $\Psi_{dm}(a, \Theta_0)$, Fig. 7c, and $T_d(a, \Theta_0)$, Fig. 7d, which are related also to the quality of the field distributions, (39) are shown.

The transit time parameter is a more usual value in the list of features for periodical structures and describes also the relative weight of the synchronous harmonic in the total distribution. Always there is a connection a smaller value of Ψ_j leads to a higher value of T_j .

For the original field component E_z the maximal phase deviation $\Psi_{zm}(a, \Theta_0)$ rises fast with Θ_0 , see Fig. 5a, and for $\Theta_0 \rightarrow \pi$ (SW mode) $\Psi_{zm}(a, \Theta_0) \rightarrow \frac{\pi}{2}$. It reflects the natural attenuation (44) for higher spatial harmonics at low values of Θ_0 . The corresponding $T_z(a, \Theta_0)$ reduction

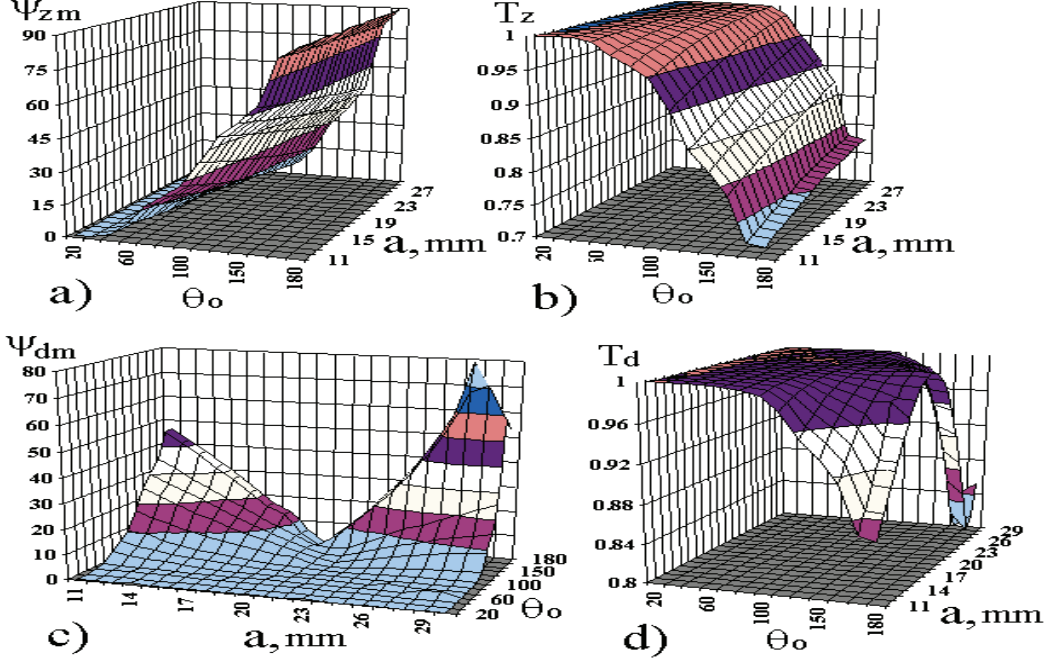


Figure 7: The surfaces $\Psi_{zm}(a, \Theta_0)$ (a), $T_z(a, \Theta_0)$ (b), $\Psi_{dm}(a, \Theta_0)$ (c) and $T_d(a, \Theta_0)$ (d) for a DLW structure, $\frac{t_d}{\lambda} = 0.054$, $\lambda = 10\text{cm}$.

can be seen in Fig. 7b and for $\Theta_0 \rightarrow \pi$, $T_z(a, \pi) \rightarrow \approx 0.75$. For larger values of aperture radii a Ψ_{zm} rises slower, also due to the stronger attenuation of higher spatial harmonics from the iris $r = a$ to the axis $r = 0$.

For small aperture radii $(\frac{a}{\lambda}) < (\frac{a}{\lambda})_{inv}$ the components of the deflecting field $e_{r0}, h_{\vartheta0}$ in a DLW have opposite phasing and the deflecting field E_d reaches smaller values of $\Psi_{dm}(a, \Theta_0)$, as compared to the original field components, Fig. 7c. It reflects the reduction of e_{dp} amplitudes, according to (34) for the opposite phasing of HE_1 and HM_1 waves. For small values of Θ_0 $\Psi_{dm}(a, \Theta_0) < \Psi_{E_{xm}, H_{ym}}(a, \Theta_0)$ because the corresponding values for contributing components are small too and additionally the compensation due to opposite E_x, H_y phasing works. This compensation essentially decelerates the rising of $\Psi_{dm}(a, \Theta_0)$ with increasing Θ_0 .

With $\Theta_0 \rightarrow \pi$ the TW mode tends to the SW with $\Theta_0 = \pi$. But the distribution of E_d for a SW mode has the properties of an 'equivalent' traveling wave, (54). For the reduction of $\Psi_{dm}(a, \Theta_0)$ both opposite phasing and the balance of the amplitudes e_{x0}, h_{y0} are essential. The second component becomes important for $\Theta_0 \approx \pi$. The balance between the amplitudes e_{x0} and h_{y0} depends on the aperture radius a , (19) and for $e_{x0} \sim -Z_0 h_{y0}$ we get $\Psi_{dm}(a, \pi) \sim 0$ instead of $\Psi_{E_x} = \Psi_{H_y} = \frac{\pi}{2}$. One can see a clear canyon in the $\Psi_{dm}(a, \Theta_0)$ surface in Fig. 7c and a corresponding arc in the $T_d(a, \Theta_0)$ surface in Fig. 7d for $\Theta_0 \rightarrow \pi$. Unfortunately, the bottom of this canyon is not so far from the curve $(\frac{a}{\lambda})_{inv}(\Theta_0)$ and not so close to the region with high values of Z_e .

5.1 Parameters for TW mode

In more details the DLW parameters for the TW mode are plotted in Fig. 8. The important TW parameter is β_g . In Fig. 8a the dependences of the aperture radius a on the operating

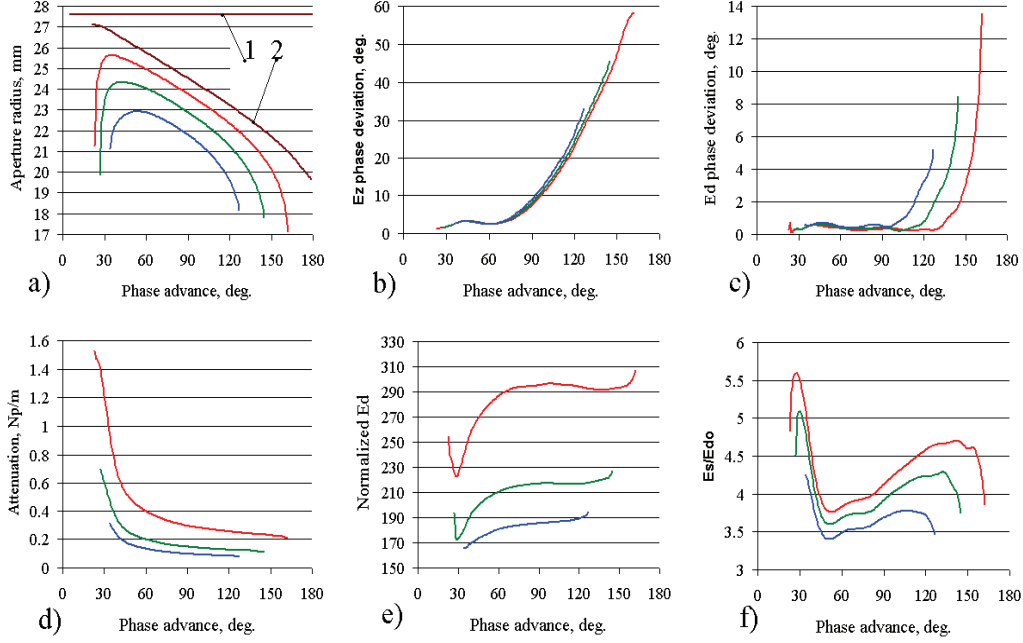


Figure 8: The dependences on Θ_0 for aperture radius a (a), the maximal phase deviation Ψ_{zm} (b), Ψ_{dm} (c), attenuation α (d), normalized field $\frac{E_{d0}\lambda}{\sqrt{P_t}}$ (e) and ratio $\frac{E_s}{E_d}$ (f) for relative group velocity values $\beta_g = -0.01$ (red curves), $\beta_g = -0.02$ (green curves) and $\beta_g = -0.03$ (blue curves).

phase advance Θ_0 is plotted as to get the required value of β_g . The brown curve (2 in Fig. 8a) shows the calculated position of the inversion point $\beta_g = 0$ in dependence on Θ_0 . According to the small pitch approximation, the inversion radius should be constant for all values of Θ_0 and $a_{inv} = \frac{\sqrt{3}}{2\pi}\lambda = 27.57\text{mm}$, (18). It is shown by the line 1 in Fig. 8a. The difference between the line 1 and the curve 2 points out the usability for the small pitch approximation.

Also in Fig. 8a are plotted the required values of a to get $\beta_g = -0.01$ (red curve), $\beta_g = -0.02$ (green curve) and $\beta_g = -0.03$ (blue curve). Other DLW parameters are plotted in Fig. 8b, f for the obtained values of a with the respective colors.

The phase deviation Ψ_{zm} (Fig. 8b) rises fast for $\Theta_0 > \frac{\pi}{2}$. Comparing plots in Fig. 8b and Fig. 8a, one can conclude, that for the condition $\beta_g = \text{const}$ lower values of Θ_0 are more important for an efficient attenuation of higher harmonics (44) in the original field components.

Due to opposite phasing of the hybrid waves, the phase deviation Ψ_{dm} for the deflecting field (Fig. 8c) rises not so fast and a low aberration level in the E_d distribution is possible for $\Theta_0 \leq \frac{2\pi}{3}$.

For small values of $\Theta_0 < \frac{\pi}{3}$ the DLW structure is closer to the small pitch approximation. The sequence of this approximation is a lower quality factor Q and a higher attenuation constant α values, Fig. 8d. The total deflecting voltage V_d (52) depends on both normalized field value $\frac{E_{d0}\lambda}{\sqrt{P_t}}$, Fig. 8e, and α . Operation with $\Theta_0 < \frac{\pi}{3}$ should be considered additionally from the point of RF efficiency.

For the electrical strength of the structure the range $45^\circ \leq \Theta_0 \leq \frac{2\pi}{3}$ is preferable, Fig. 8f.

5.2 Parameters for SW mode

Parameters of the DLW structure for SW mode are plotted in Fig. 9.

The effective shunt impedance Z_e decreases with increasing a , Fig.9a, and the maximal electric

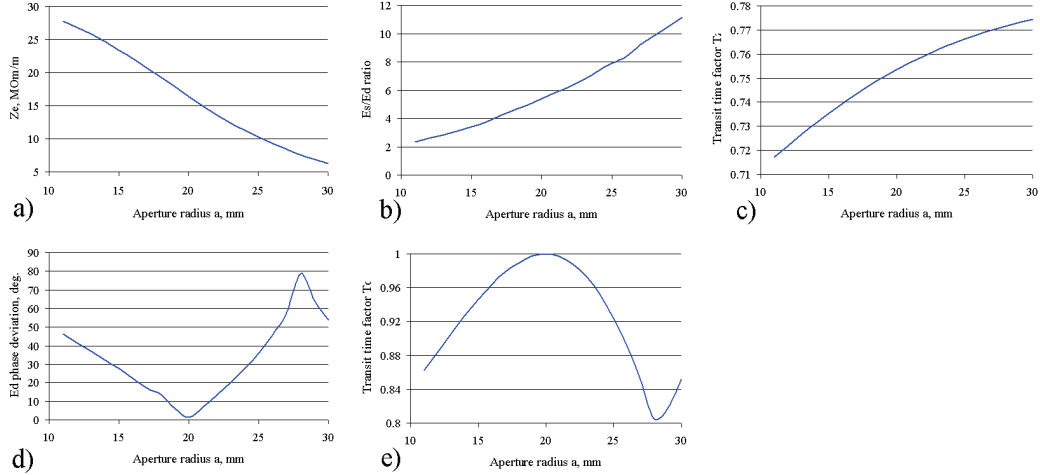


Figure 9: The parameters of the DLW structure for SW mode in dependence on aperture radius. Effective transverse shunt impedance Z_e (a), ratio $\frac{E_s}{E_d}$ (b), transit time factor T_z (c), the maximal phase deviation Ψ_{dm} (d) and transit time factor T_d (e) for the deflecting field.

field at the surface increases, Fig. 9c. The maximal phase deviation Ψ_{zm} for the longitudinal E_z component is always $\Psi_{zm} = \frac{\pi}{2}$, due to the step-wise rise in the E_z phase in SW mode and T_z is always $T_z \simeq 0.75$, Fig. 9c.

For the deflecting field E_d the value of the phase deviation Ψ_{dm} depends on the amplitude balance of e_{x0} and h_{y0} , Fig. 9d, which defines also the value of $T_d \sim 1$, Fig. 9e. We can get $\Psi_{dm} \approx 0$, see Fig. 9d, at some value of a_0 , but it is close to the position of the inversion point. For DLW in SW mode with $\Psi_{dm} \approx 0$ exist limitations from the mode mixing problem as described below

As it was shown in Section 4.3, the SW operating mode is more efficient for obtaining a required value of V_d with a short DS. As for the homogeneity of the longitudinal component E_z , essential reductions of aberrations (reduction of higher spatial harmonics) can not be realized for SW mode. As for aberrations in the transverse field E_d , we have a contradictory choice for DLW - either RF effective operation with smaller E_s values, but significant level of nonlinear additions, or operation with reduced aberrations at the expense of RF power and at higher surface field.

6 Parameters of the decoupled TE-structure

In DLW structures the aperture radius a defines simultaneously both RF efficiency, and dispersion properties. In TE-structures (Fig. 1d) these parameters are separated. The RF efficiency depends mainly on the distance between the noses (effective aperture radius) and the disk thickness. The passband width can be changed by the inner disk radius r_w . This structure has no rotational symmetry. For the complete description of the field distribution, starting from (2), we have to add waves and harmonics with $n = 3, 5, 7, \dots$ variations along azimuth, see Section 3.3. Below we do however not consider multipole additives. The nose tip shape was

optimized to reduce the multipole additives and this shape was used for consideration. The study of the RF parameters has been performed in a range of $\frac{\pi}{9} \leq \Theta_0 \leq \pi$ and $0.06 \leq \frac{a}{\lambda} \leq 0.15$, assuming $\lambda = 10\text{cm}$ with all other parameters - the disk thickness $t_d \approx 0.52d$ and iris radius $\frac{r_w}{\lambda} = 0.24$ fixed from the previous RF efficiency optimization.

Results are presented in Fig. 10 as two dimensional surfaces. The range of aperture radii,

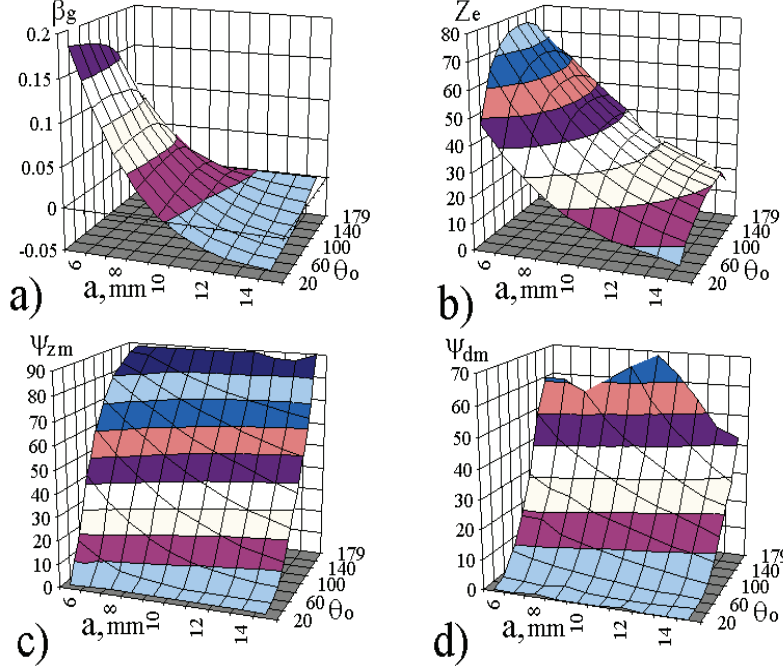


Figure 10: The surfaces of $\beta_g(a, \Theta_0)$ (a), $Z_e(a, \Theta_0)$ (b) $\Psi_{zm}(a, \Theta_0)$ (c) and $\Psi_{dm}(a, \Theta_0)$ for the TE-structure, $\lambda = 10\text{cm}$.

considered for the TE-structure and DLW, have a common region $0.11 \leq \frac{a}{\lambda} \leq 0.15$. It allows us to compare the general behavior of structure parameters both qualitatively and quantitatively. For small aperture radii $\frac{a}{\lambda} \leq 0.11$ the structure has equal phasing of the synchronous harmonics e_{x0}, h_{y0} and, as a consequence, a positive group velocity $\beta_g > 0$, Fig. 10a, which decreases with aperture increasing radius. Also for each value of Θ_0 we find the inversion point $(\frac{a}{\lambda})_{inv}(\Theta_0) \approx 0.11$, corresponding to $\beta_g = 0$. Above the inversion point $\beta_g < 0$ and with further increasing $\frac{a}{\lambda}$ the TE-structure degenerates into a DLW.

For small aperture radii the TE-structure reaches high values of Z_e , Fig. 10b, which decrease with increasing a . For the same aperture radius both TE-structure and DLW have approximately equal values of Z_e , but differ strongly in the width of the passband.

Similar to a DLW, see Fig. 7a, the phase deviation $\Psi_{zm}(a, \Theta_0)$ rises with Θ_0 , Fig. 10c, but the rise is faster - for smaller values of a the attenuation of higher harmonics in TE-structures, according to (44), is not so strong.

For equal e_{x0}, h_{y0} phasing the phase deviations $\Psi_{dm}(a, \Theta_0)$ for the deflecting field E_d is larger than for the E_x, H_y components and rises faster with Θ_0 for small values of a . According to (34), the amplitudes of the spatial harmonics in the E_d description, are enlarged for equal phasing of HE_1 and HM_1 waves as compared to opposite phasing.

For values of a above the inversion point the harmonics e_{x0} and h_{y0} obey an opposite phasing and the partial compensation starts, leading to a reduction of $\Psi_{dm}(a, \Theta_0)$, which is however

not very effective. For the compensation of the harmonics both opposite phasing and comparable values for amplitudes are essential. In the TE-structure with introduced noses, for the considered range of parameters, the amplitude of e_{x0} dominates with respect to the amplitude of $Z_0 h_{y0}$ and the phase deviation $\Psi_{dm}(a, \Theta_0)$ for the E_d is defined mainly by $\Psi_{xm}(a, \Theta_0)$ for the E_x component, Fig. 10d, which rises with Θ_0 as all original field components. In the considered range of parameters this is the reason for the absence of a canyon in the dependence of $\Psi_{dm}(a, \Theta_0)$ on a for $\Theta_0 \sim 180^\circ$, as we have seen for the DLW structure in Fig. 7c, Fig. 9d.

6.1 Parameters for TW mode

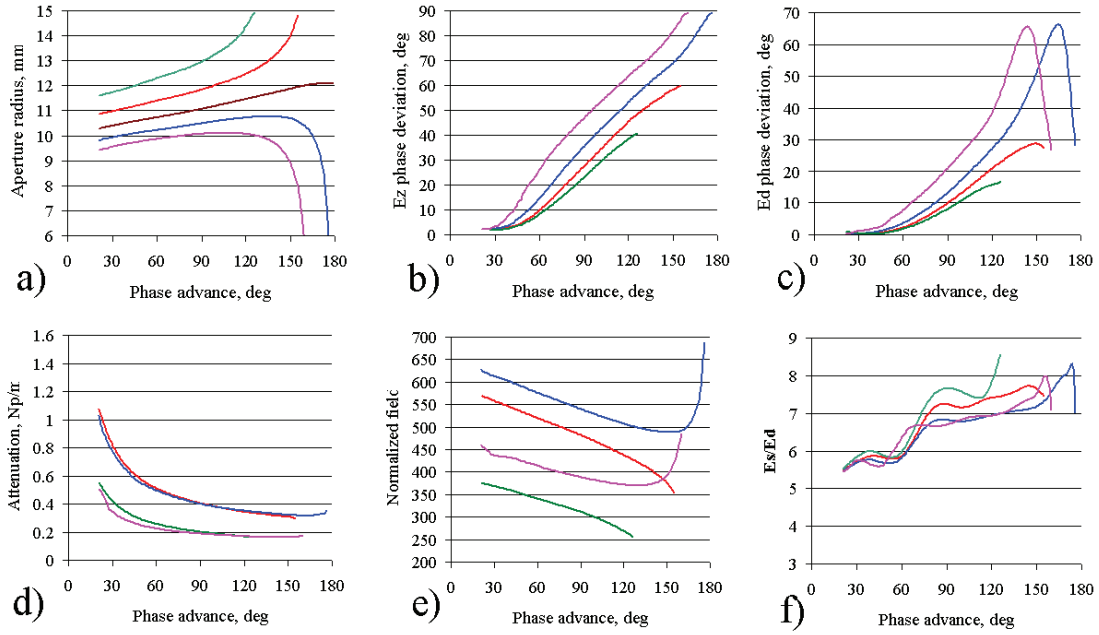


Figure 11: The dependences on Θ_0 on the aperture radius a (a), the maximal phase deviation Ψ_{zm} (b), Ψ_{dm} (c), attenuation α (d), normalized field $\frac{E_{z0}\lambda}{\sqrt{P_t}}$ (e) and ratio $\frac{E_s}{E_d}$ (f) for relative group velocity values of $\beta_g = -0.01$ (red curves), $\beta_g = 0.01$ (blue curves), $\beta_g = -0.02$ (green curves) and $\beta_g = 0.02$ (magenta curves).

Regarding RF efficiency in the TW mode, small values of a are not attractive, because they result in high values of β_g and related lower values of normalized field $\frac{E_{z0}\lambda}{\sqrt{P_t}}$. The inversion of the sign of β_g allows, similar to the DLW, a reasonable choice of β_g . The dependence of the inversion value $(\frac{a}{\lambda})_{inv}$ on Θ_0 is shown in Fig. 11a with a brown curve.

Parameters of the TE-structure for TW mode are plotted in Fig. 11 in the same style with equivalent parameters as for the DLW in Fig. 8. Comparing the plots in Fig. 10b, c and Fig. 8b, c, one can see for the same value of β_g larger phase deviations $\Psi_{zm}(a, \Theta_0)$ for E_z , Fig. 11b, Fig. 8b, and essentially larger phase deviations $\Psi_{dm}(a, \Theta_0)$ for E_d , Fig. 11c, Fig. 8c in the TE-structure. These results are the consequences of small values of a and equal phasing of e_{x0} and h_{y0} .

As compared to a DLW, the structure has a lower Q -factor, resulting in a higher attenuation constant α , as one can see by comparing the plots in Fig. 11d and Fig. 8d. But the normalized

field $\frac{E_{d0}\lambda}{\sqrt{P_t}}$ (59) is essentially higher, see plots in Fig. 11e and Fig. 8e. The total deflecting voltage \dot{V}_d depends on the normalized field, the attenuation constant and the structure length L (60). Instead of a higher α , the reserve in the value of $\frac{E_{d0}\lambda}{\sqrt{P_t}}$ is sufficient to find values of L with higher RF efficiency. As one can see from Fig. 11e, f, regarding RF efficiency a TW operation with $\beta_g > 0$ is preferable - as compared to $\beta_g < 0$ a higher value $\frac{E_{d0}\lambda}{\sqrt{P_t}}$ is reached for the same α . But the phase deviations, both Ψ_{zm} and Ψ_{dm} , are larger for $\beta_g > 0$, see Fig. 11b, c.

Due to the noses and, especially, the nose end shape, TE-structures reach higher $\frac{E_s}{E_d}$ ratios, see Fig. 11e and Fig. 8e. Generally, DS's with equal E_x and H_y phasing should have higher values of the ratio $\frac{E_s}{E_d}$. The maximal electric field at the surface E_s is connected with E_x . For the opposite phasing of the e_{x0} and h_{y0} components E_x and H_y contribute together, (21) to the creation of E_d . For equal e_{x0}, h_{y0} phasing the magnetic field partially compensates the deflection from the electric field and a higher value of E_x is required to produce the same deflecting effect.

6.2 Parameters for SW mode

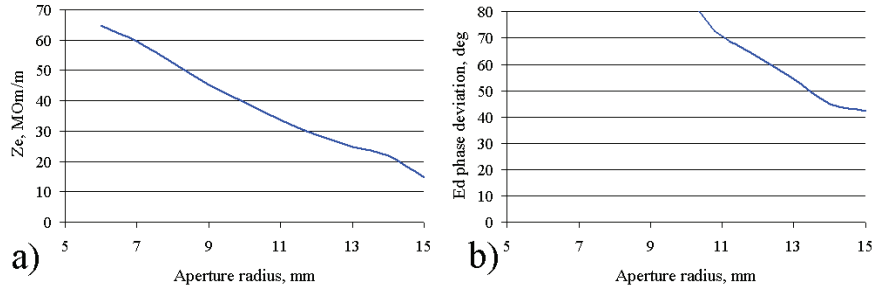


Figure 12: The shunt impedance Z_e (a) and the maximal phase deviation Ψ_{dm} (b) for SW mode in dependence on the aperture radius a .

Due to higher values of Z_e , Fig. 12a, SW mode was originally proposed as preferable application of TE-structures. As compared to a DLW, a decoupled TE-structure has additional freedom in the dimensions - nose opening along azimuth and inner disk radius, which differs from the aperture radius. The cell dimensions were optimized for RF efficiency assuming an L-band operation with $a = 15.5mm$, corresponding to $a = 6.72mm$ in the S-band range.

The phase deviation Ψ_{zm} shows a typical SW mode behavior at $\Psi_{zm} = \frac{\pi}{2}$. Concerning the deflecting field E_d the dependence of Ψ_{dm} on a is more interesting, Fig. 12c. In the range $5mm < a < 11mm$ (below the inversion point), hybrid waves have equal phasing; the 'equivalent' traveling wave in (54) is the backward wave with respect to the particle motion and $\Psi_{dm} \approx \frac{\pi}{2}$. Above the inversion point $a > 11mm$ we find a negative structure dispersion, opposite e_{x0}, h_{y0} phasing and Ψ_{dm} decreases with further increasing a . If the plot of Ψ_{dm} in Fig. 12b would be continued to $a \approx 20mm$, a second inversion point and a valley in the plot of Ψ_{dm} would appear, similar to the valley in the plot of Ψ_{dm} for the DLW in Fig. 9d, because the TE-structure degenerates in its properties to a DLW for large values of a .

The decoupled TE-structure has been considered here mainly in contrast to a DLW. For a small aperture radius this DS shows an equal e_{x0}, h_{y0} phasing, a high RF efficiency, but a poor deflecting field quality for bunch rotation. In the DLW consideration the necessity of opposite e_{x0}, h_{y0} phasing was illustrated to achieve a high quality of the deflecting field, but at the

expense of RF efficiency.

The main value of this study is the detection of the dispersion inversion at a small aperture radius. After that the advantage of the decoupled control over the field distribution was used to combine RF efficiency and deflecting field quality, [14].

7 Hybrid waves phasing and balance.

In the following plots for field distributions are shown to compare the effect of both the opposite and the equal phasing of e_{x0} and h_{y0} .

A DS with a total length of $200\text{mm} = 2.0 \cdot \lambda$ is considered for operation in TW and SW mode with the same average deflecting field of $E_{d0} = 1\text{MV/m}$. To emphasize the particularities in distributions, some frames in plots have different scales of the field strength.

In Fig. 13 plots of distributions for opposite e_{x0}, h_{y0} phasing are shown, for a DLW structure

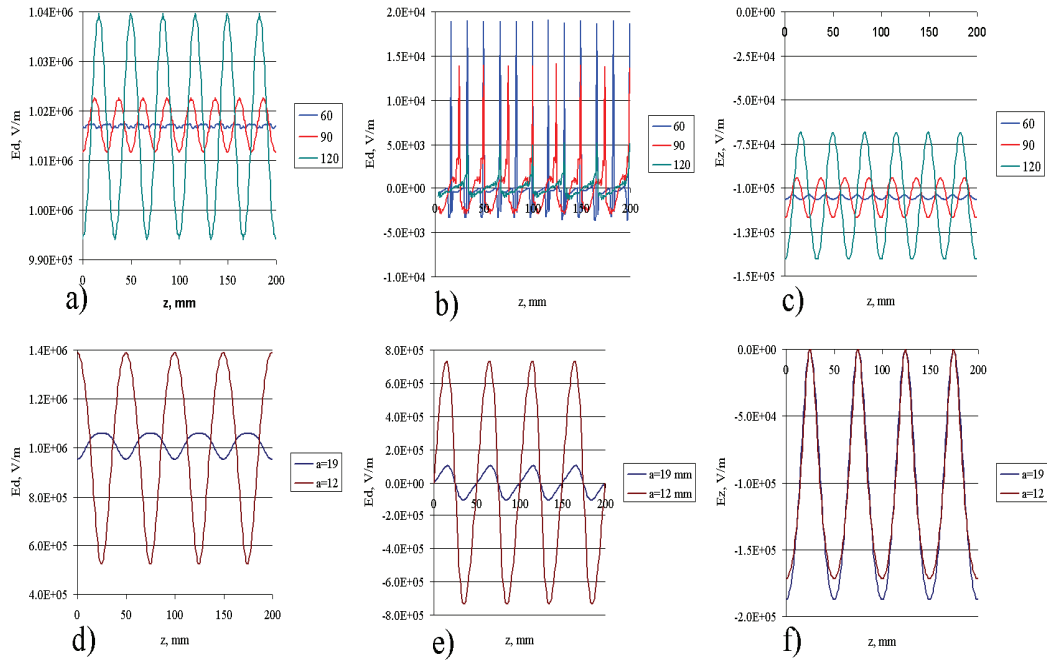


Figure 13: Plots of E_d and E_z distributions for DLW TW (upper row) and SW mode (bottom row). TW mode with $\Theta_0 = \frac{\pi}{3}, \frac{\pi}{2}, \frac{2\pi}{3}$ - blue, red and green curves, respectively. SW mode for $\frac{a}{\lambda} = 0.12, 0.194$, brown and dark blue curves, respectively. The plotted distributions show $E_d, \phi = 0$, (a), (d) - $E_d, \phi = \frac{\pi}{2}$, (b), (e) and $E_z, \phi = \frac{\pi}{2}$ (c), (f).

with large aperture radius $\frac{a}{\lambda} \sim 0.23$. A detailed description of the plots is given in the caption of Fig. 13. For direct comparison equivalent plots are shown in Fig. 14 for the decoupled TE structure with equal e_{x0}, h_{y0} phasing and small aperture radius $\frac{a}{\lambda} \sim (0.07 - 0.11)$. In addition to plots for equal phasing, corresponding to $\beta_g > 0$, plots for opposite phasing, i.e. $\beta_g < 0$ are presented in Fig. 14. Numerical data - amplitudes of the spatial harmonics, calculated according (43) - are presented in the Table 3.

Comparing the distributions of the original field component E_z for TW mode, $\Theta_0 = \frac{\pi}{3}$, in Fig. 13c, Fig. 14c and the e_{zp} coefficients in the Table 3, we see the effect of a large aperture radius,

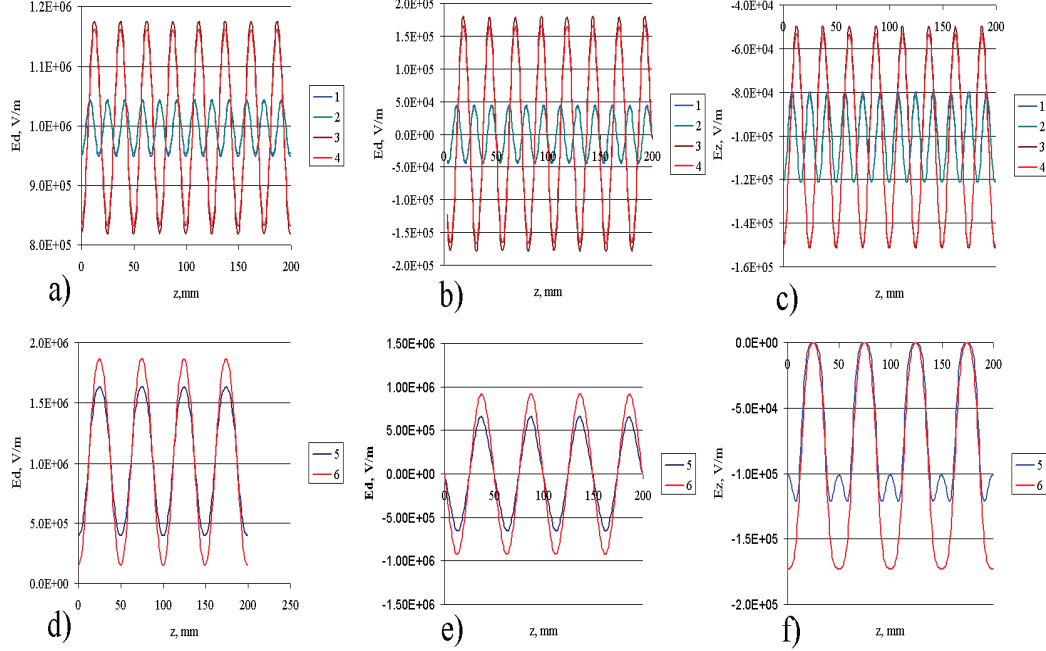


Figure 14: Plots of E_d and E_z distributions in the decoupled TE structure for TW (upper row) and SW (bottom row) operation. TW mode with $\Theta_0 = \frac{\pi}{3}, \beta_g = -0.01$, $\Theta_0 = \frac{\pi}{3}, \beta_g = 0.01$, $\Theta_0 = \frac{\pi}{3}, \beta_g = -0.02$ and $\Theta_0 = \frac{\pi}{2}, \beta_g = 0.02$ - blue, red, green and brown curves, respectively. SW mode for $\frac{a}{\lambda} = 0.0672, 0.108$ - dark blue and red curves, respectively. The plotted distributions show $E_d, \phi = 0$, (a), (d) - $E_d, \phi = \frac{\pi}{2}$, (b), (e) and $E_z, \phi = \frac{\pi}{2}$ (c), (f).

which provides a stronger attenuation of harmonics toward the axis, (44). The amplitudes of higher harmonics in e_{zp} are essentially smaller in DLW. With increasing Θ_0 the amplitudes of harmonics in the original field components at the axis rise due to weaker attenuation.

For the deflecting field E_d we directly see from Fig. 13 a, b, Table 3, a reduction of harmonic amplitudes $|e_{dp}| \ll |e_{zp}|$, as compared to the original field components, for opposite e_{x0}, h_{y0} phasing both for bunch deflection $\phi = 0$ and for bunch rotation $\phi = \frac{\pi}{2}$. The spikes in Fig. 13b ($E_d, \phi = \frac{\pi}{2}$) reflect just numerical noise in the simulation of the fields; the regular effects in the deviations of E_d are much below the noise. According to (34), for opposite phasing of HE_1 and HM_1 waves in the field description (16) the higher spatial harmonics in the E_x and H_y components compensate each other on the background of an increased total main harmonic.

For equal e_{x0}, h_{y0} phasing we do not see, Fig. 14 a, b, Table 3, a reduction of the harmonics amplitudes in E_d in comparison with the original field components.

The advantage of opposite e_{x0}, h_{y0} phasing for the suppression of harmonics is especially brightly shown in the TW mode in Fig. 14 a, b, c - for the negative group velocity (opposite phasing) the deviation from the average (due to the higher spatial harmonics) is always larger, as compared to the same value but positive group velocity (equal phasing).

For a TW mode with low value of $\Theta_0 \leq \frac{\pi}{2}$ the amplitude balance $|\frac{Z_0 h_{y0}}{e_{x0}}|$ is not of primary importance - for harmonics suppression in the deflecting field the attenuation (44) in original field components is more essential. The plots of the $\frac{h_{y0}}{e_{x0}}$ balance are given in Fig. 15a together with the corresponding plots of Ψ_{dm} both for TW and SW mode. The black dotted curve in Fig. 15a shows the plot of the $\frac{Z_0 h_{y0}}{e_{x0}}$ balance in a DLW according to the small pitch approximation,

Table 3: The relative amplitudes for higher spatial harmonics in the field distributions for the DLW and decoupled TE structures.

DS, Operation, $a =, mm$	Θ_0	$E_z,$ e_{z1}	$E_z,$ e_{z2}	$E_z,$ e_{z3}	$E_d,$ e_{d1}	$E_d,$ e_{d2}	$E_d,$ e_{d3}
DLW,TW,23.80mm	60	-0.0048	-0.0007	-0.0010	0.0006	-0.0009	0.0006
DLW,TW,23.58mm	90	-0.0581	-0.0004	-0.0003	0.0009	-0.0001	-0.0001
DLW,TW,22.33mm	120	-0.1950	-0.0048	0.0001	0.0020	-0.0015	0.0012
DLW,SW,12.0mm	180	-0.6103	-0.1385	-0.0348	-0.3818	-0.0623	-0.0008
DLW,SW,19.4mm	180	-0.5619	-0.0691	-0.0077	-0.0271	-0.0148	0.0047
TE-,TW,10.45mm	60	-0.1131	-0.0002	0.0000	0.0227	-0.0001	0.0002
TE-,TW,11.39mm	90	-0.2520	-0.0024	0.0006	0.0896	0.0002	-0.0001
TE-,SW,6.72mm	180	-0.5178	0.0998	0.1165	-0.3010	-0.0194	0.0124
TE-,SW,10.08mm	180	-0.4842	0.0640	0.0472	-0.4384	-0.0064	0.0076

(19). As can be seen from Fig. 15b, for a DLW in TW mode with $\Theta_0 = \frac{\pi}{3}$ the phase deviations Ψ_{dm} are very small for all values of the aperture radius a , even though the harmonic amplitudes $Z_0 h_{y0}$ and e_{x0} are not balanced, Fig. 15a.

The role of the balance of $\frac{Z_0 h_{y0}}{e_{x0}}$ increases with $\Theta_0 \rightarrow \pi$ and for a SW operation it is the only

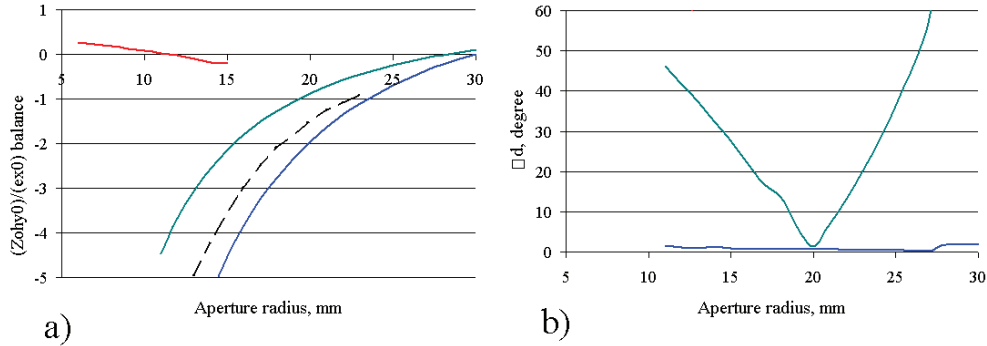


Figure 15: Plots of $\frac{Z_0 h_{y0}}{e_{x0}}$ balance (a) and corresponding plots of Ψ_{dm} (b) for a DLW in TW mode ($\Theta = \frac{\pi}{3}$, blue curves) and SW mode, green curves. The red curve represents the balance of $\frac{Z_0 h_{y0}}{e_{x0}}$ for a decoupled TE-structure in SW mode.

way to suppress harmonics in a deflecting field. The aperture radius $\frac{a}{\lambda} = 0.194$ for a DLW in SW mode corresponds to the minimal value of phase deviation of $\Psi_{dm} \approx 1.8^\circ$ and $\frac{Z_0 h_{y0}}{e_{x0}} \approx -0.85$, Fig. 15b,c. Comparing the amplitudes e_{dp} in the Table 3 for $\frac{a}{\lambda} = 0.12$ and $\frac{a}{\lambda} = 0.194$, one can see a reduction of e_{d1} by more than an order of magnitude and a reduction of e_{d2} by more than a factor of four. But the deflecting field deviations are suppressed for $\frac{a}{\lambda} = 0.194$ in 'total, i.e. on the background of the first harmonic e_{d1} which is reduced by one order of magnitude we see in the distribution of the second harmonic $E_d, \phi = \frac{\pi}{2}$ in Fig. 13e $e_{d2} - E_d$ non symmetric deviations.

Differing from the prediction of $e_{dxp}(x, y) \approx 0$ for $A = -B$, (34), the results of the numerical simulations show for a SW mode a minimal value $\Psi_{dm} \approx 2^\circ$ at $B \approx -0.87 \cdot A$. In this case we realize a DS option with damped e_{dp}^o terms in (53), when the not compensated contribution of $e_{r0} + Z_0 h_{\theta 0}$ to the oscillations in (52) from the synchronous harmonics in E_r and H_θ is damped

by the first harmonics $e_{r1} + Z_0 h_{\theta 1}$ and simultaneously the amplitudes for higher harmonics in E_d are reduced, according to (34).

7.1 Structures classification

The classification of a structure with a complicated field distribution is always rather conditional. Often the visual characteristics of the structure or field distribution are used. For example, the DS with evidently dominating transverse electric field, Fig. 1d, was treated in [4] as TE-type. In Fig. 16 it is shown, how this DS can be continuously transformed, with an appropriate transformation of the field distribution, into other DS's.

Suppose the starting point is (b) in Fig. 16 - the original DS option, described in [4]. By reducing the iris radius $r_w \rightarrow a$ we come through Fig. 15c, Fig. 15d to Fig. 15e - the well known DLW. In this way an equal e_{x0}, h_{y0} phasing changes into an opposite phasing. Transformation into another direction $r_w \rightarrow b$ leads to other structures, Fig. 15 a, which are very compact, $2b \leq \frac{\lambda}{2}$, have a high value of Z_e in SW π mode and an equal e_{x0}, h_{y0} phasing, similar to the initial Fig. 15b option. The deflecting field distribution in such structures is described by (53), and looks similar as the plots in Fig. 14 d, e. In such structures, Fig. 15a, the central bunch particle will receive, both for bunch deflection and for bunch rotation, a strong oscillating impact, comparable to the average deflecting field, and can thus be displaced to a region with strong nonlinear additions in the field. Application of these structures for heavy ions is tolerable due to the small transverse dimensions at low frequencies, [16]. Moreover, for $\beta \ll 1$ the magnetic component in the deflecting force is reduced and there is no substantial difference between opposite and equal e_{x0}, h_{y0} phasing in (52). For bunch rotation at $\beta \sim 1$, especially for multiple bunch passages, such DS's should be considered more carefully. With a small deterioration of the transverse emittance in each DS passage, the danger of cumulative emittance growth in the multiple passages appears.

It the previous consideration we have seen the importance of the e_{x0}, h_{y0} phasing and balance

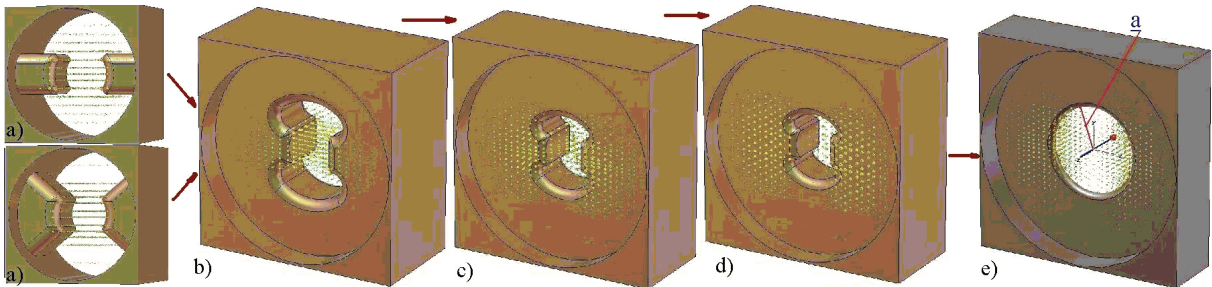


Figure 16: Transformation of deflecting structure.

for the deflecting field quality. Most important is the phasing. For TW mode we can have always a tolerable field quality for low Θ_0 , but opposite e_{x0}, h_{y0} phasing leads to a better E_d distribution, regardless of the $\frac{Z_0 h_{y0}}{e_{x0}}$ balance. For a SW mode the opposite e_{x0}, h_{y0} phasing also leads first to a better E_d distribution and allows (second) to reduce aberrations in E_d for the appropriate $\frac{Z_0 h_{y0}}{e_{x0}}$ balance.

With respect to the deflecting field quality, it looks attractive to distinguish all DS in two groups - with opposite and with equal hybrid waves HE_1, HM_1 phasing. But hybrid waves HE_1 and HM_1 are special functions, practically inaccessible to a visual perception. We can define the

phasing and the balance from the results of a treatment for the simulated field distribution, but it is not clear.

Suppose we have a DS with a pronounced predominance of the transverse electric field in the aperture $\vec{E} \approx \vec{i}_x E_x \approx \vec{i}_r E_r$, for example the DS, shown in Fig. 1b, Fig. 1d or Fig. 15a. From the Maxwell equation $\text{rot}\vec{E} = -\frac{\partial\vec{B}}{\partial t}$ for the synchronous harmonics in (2) for each field component we find:

$$-ikZ_0 h_{\vartheta 0}(r, z) = \frac{\partial e_{r0}(r, z)}{\partial z} - \frac{\partial e_{z0}(r, z)}{\partial r}, \Rightarrow Z_0 h_{\vartheta 0}(r) = \frac{k_{z0}}{k} e_{r0}(r) - \frac{i}{k} \frac{\partial e_{z0}(r)}{\partial r}. \quad (62)$$

All DS with a pronounced predominance of the transverse electric field in the aperture $|E_x| \gg |E_z|$ have an equal phasing of the hybrid waves HE_1 and HM_1 . This is valid also for DS with rods and DS utilizing a TM_{010} mode in combination with a transversely passing bunch.

To have an opposite phasing for the hybrid waves HE_1 and HM_1 , in the distribution of the original electric field the E_z component should dominate, as one can see it in Fig. 1a, Fig. 1c and Fig. 15c.

8 End cell problem

In periodical structures with a finite length the natural boundary conditions are magnetic or electric wall conditions at the planes of mirror symmetry. The practical case are electric conditions in the middle plane between adjacent disks. In this case the distributions for the field components in a SW cavity are perfectly the same as for a periodical structure.

In a real DS perfect boundary conditions are not possible at the ends of the structure - always a beampipe is required. The field penetrating into the beampipe decays away from the structure but provides an initial transverse kick, which starts before the particles enter the actual structure. The field distribution in the beampipe is not controllable and in order to reduce this part of the deflection and thus simultaneously reduce the total input kick the beampipe radius r_t should be as small as reasonably possible.

8.1 End cell for SW mode

A model for the definition of the end cell in a SW cavity is shown in Fig. 17. The end cells together with the beampipe are tuned to the operating frequency as separate units by adjusting the cell radius r_{ce} while keeping the boundary condition $E_\tau = 0$ in the middle of the iris connecting to the periodic structure. This ensures that the frequency and the field distribution are independent of the number of regular cells in the cavity.

By changing the length L_e of the end cell the distribution of $E_d, \phi = \frac{\pi}{2}$ can be changed in a wide range, Fig. 18. The transverse field can be reduced but does not disappear completely. In order to reduce the input kick the minimization of the phase deviation from the synchronous particle, following to (54) is possible. But another procedure is more convenient for a SW mode, [14].

The first integral $Int_{1t}(z)$

$$Int_{1t}(z) = \int_{-\infty}^z E_d(z', \phi = \frac{\pi}{2}) dz'. \quad (63)$$

is proportional to the transverse momentum and thus the transverse velocity of a particle, which defines the direction of the particle motion. Equivalently we can calculate the second integral $Int_{2t}(z)$, which is proportional to the transverse displacement of a particle. By varying

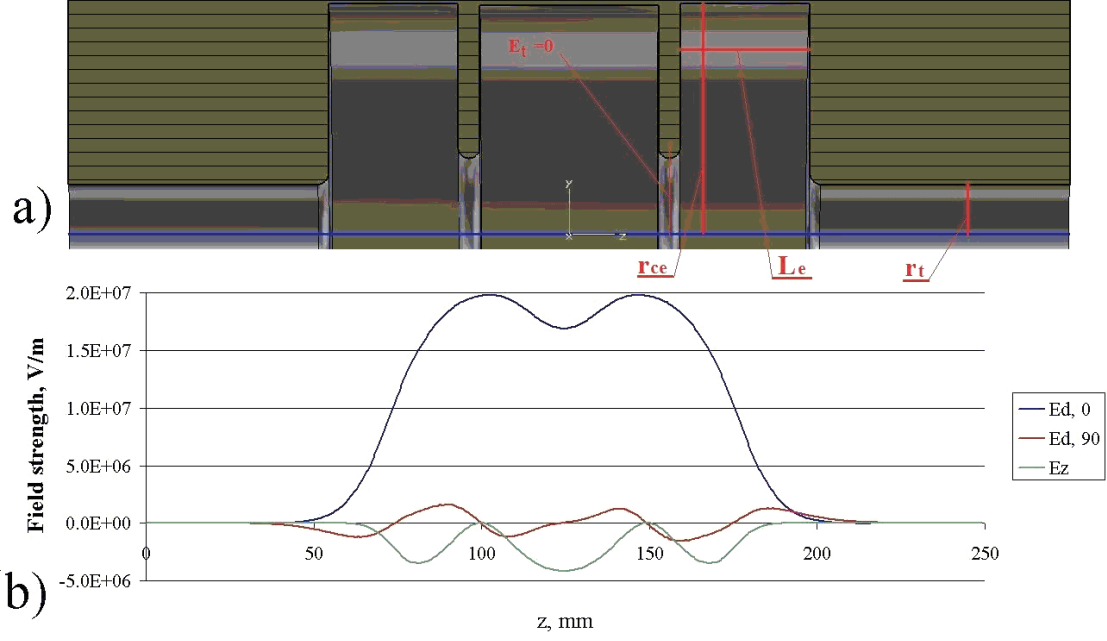


Figure 17: Model for the definition of the end cell (a) and distributions for field components (b) - $E_d, \phi = 0$ (blue curve), $E_d, \phi = \frac{\pi}{2}$ (red curve) and $E_z, \phi = \frac{\pi}{2}$ (green curve).

the end cell length L_e we can control either the central particle direction or displacement at a specified point.

The final field distributions, shown for three a cell cavity in Fig. 17b, are obtained from the condition $Int_{1t}(z) = 0$ at the position of the first iris, i. e. the particle enters the regular cavity part parallel to the axis. It is realized for $L_e + \frac{td}{2} \approx \frac{d}{2}$ - the length of the end cell is approximately half of the structure period.

The condition $Int_{1t}(z) = 0$ results in a reduced variation of $E_d, \phi = \frac{\pi}{2}$ in the end cell, comparable to the residual $E_d, \phi = \frac{\pi}{2}$ variation in the regular structure and keeps the central particle near the DS axis.

8.2 End cell for TW mode

The end cell problem for a TW mode requires a more difficult technique, because the end cell is simultaneously the RF coupler cell. Additionally to the task of reducing the input kick we have the task of RF matching.

For a TW mode the input kick in the end cell is described by phase deviations in the deflecting field distribution, (56) and the kick minimization is equivalent to the $|d\psi_d(z)|$ minimization in the end cell. For this purpose the method calculations of reflection coefficients for RF coupler matching at $\phi = 0$, [15], has been extended for simultaneous $d\psi_d(z)$ determination at $\phi = \frac{\pi}{2}$.

In Fig. 19 the distributions of E_d and E_z are plotted for a DLW in TW mode, $\Theta_0 = \frac{\pi}{3}$. Comparing with the corresponding plots in Fig. 3, one can see, at first, essentially reduced variations of E_d and E_z inside the regular structure for $\Theta_0 = \frac{\pi}{3}$. It is the consequence of stronger harmonics attenuation for lower Θ_0 . But, on the background of reduced aberrations in the regular structure, the input kick is clearly visible.

Similar to the SW case, the input kick already starts in the beampipe. It is not a controllable

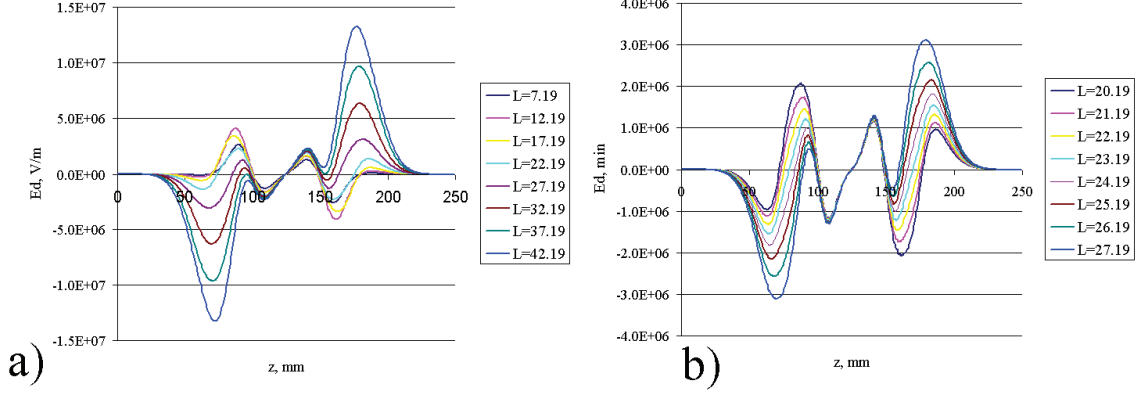


Figure 18: Examples of input kick control in a wide range (a) and for more precise compensation (b) by the choice of the end cell length L_e .

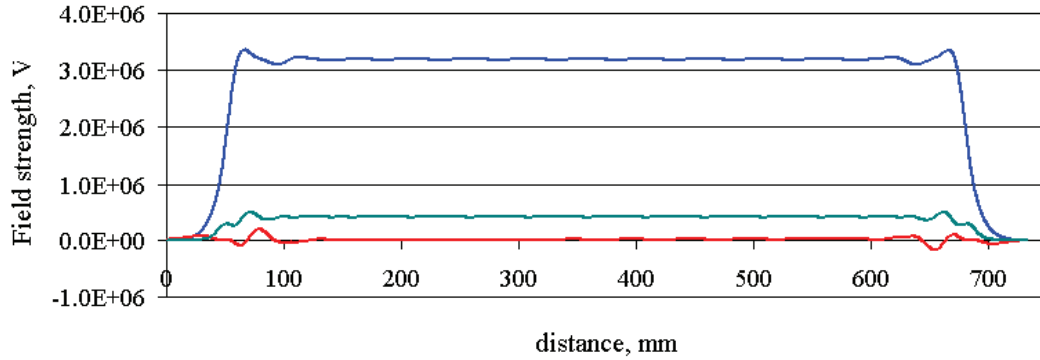


Figure 19: Plots of E_d and E_z distributions for a DLW in TW mode, $\Theta_0 = \frac{\pi}{3}$. The plots are - $E_d, \phi = 0$ - blue curve, $E_d, \phi = \frac{\pi}{2}$ - red curve and $E_z, \phi = \frac{\pi}{2}$ - green curve.

region and the only way to reduce the kick is the reduction, if possible, of the beampipe radius. For a large beampipe radius the value of the first integral (63) over the beam pipe region is essentially large and some times it is not so easy to compensate it with the end cell only.

The most essential parameter for the value of the input kick is the length of the end cell, similar to the SW case, and the minimal kick values are obtained for an end cell length of $\approx 0.5d$. The plots of the field component distributions in Fig. 19 and Fig. 5 correspond to the half cell RF couplers.

For the DS with visible E_d deviations, Fig 5, $\Theta = \frac{2\pi}{3}$, it is not a big problem to reduce the input kick to the level of the E_d deviations in the regular part of the DS. If we use a DS with a more uniform field distributions, $\Theta = \frac{\pi}{3}$, Fig. 19, the input kick is a single source for a field nonlinearity and we see an additional effect of the RF coupler cell - as the deterioration of the periodicity the RF coupler perturbs the phase distribution in the adjacent DS cells. In Fig. 19 the maximal value of $E_d, \phi = \frac{\pi}{2}$ is displaced from the structure ends to the adjacent DS cells, even though the dimensions of these cells are unchanged. This effect needs more study.

The distribution of $E_d(z, \phi = \frac{\pi}{2})$ is always an odd function with respect to the DS middle. This means, that $Int_{1t}(z)$ and $Int_{2t}(z)$ are always even and odd, respectively, functions with respect to the DS middle.

9 Dispersion properties and limitations

In periodical structures the main spatial harmonics provide flux propagation of the the RF power. In most cases the opposite $e_{r0}, h_{\vartheta0}$ phasing at the DS axis results in a negative value of β_g . This is not the same statement. The opposite $e_{r0}, h_{\vartheta0}$ phasing at the DS axis definitely means a part of the RF power P_{tr}^- in the nearest vicinity of the axis, propagates into negative direction. But the distribution of the field components depends on the radius r which can result in a part of the RF power P_{tr}^+ propagating into positive direction near $r \sim a$. The sign and the value of the group velocity depends on the total flux $P_{tr}^{tot} = P_{tr}^+ + P_{tr}^-$. By changing the aperture radius in a DLW we change the ratio $\frac{P_{tr}^-}{P_{tr}^+}$ and for $P_{tr}^- + P_{tr}^+ = 0$ β_g inversion is reached, (18). The inversion phenomenon is the consequence of the field distribution in the hybrid waves HE_n and HM_n , even for a single passband, when mode mixing effects are absent. Together with more flexibility, the inversion phenomenon and, mainly, the dependence of the inversion point on Θ_0 , provides some limitations on the choice of the DS dimensions.

In Fig. 20a the plots of the dependence of aperture radius a on Θ_0 to get a required value

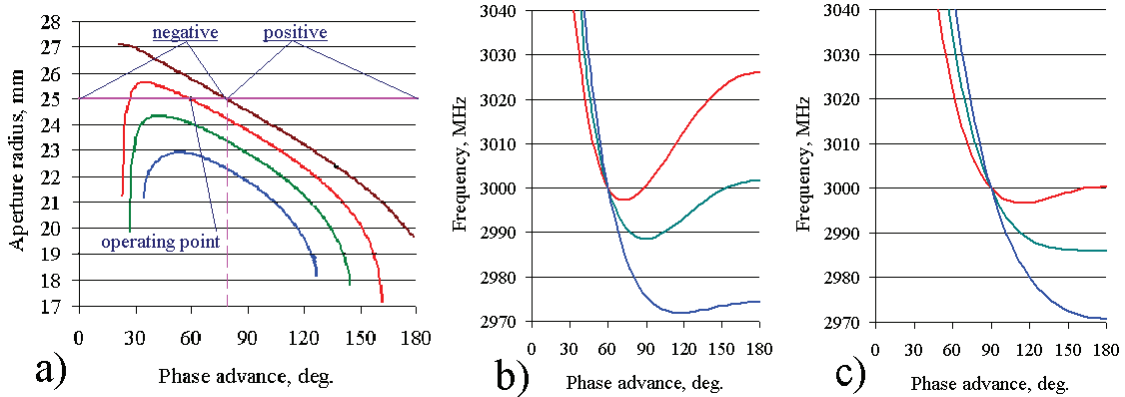


Figure 20: The dependences of the aperture radius a on Θ_0 (a) and the dispersion curves for the DLW TW structure with $\Theta_0 = \frac{\pi}{3}$ (b) and $\Theta_0 = \frac{2\pi}{3}$ (c) corresponding to $\beta_g = -0.01, -0.02, -0.03$, red, green and blue curves, respectively.

of β_g for a DLW in TW mode is reproduced from Fig. 8a. The inversion point dependence is plotted in Fig. 20a by a brown curve. In Fig. 20 b, c the dispersion curves for a DLW with different values of Θ_0 and β_g are plotted. As one can see from Fig. 20 b, some curves have a complicated behavior - the tail of the dispersion curve at $\Theta \rightarrow \pi$ goes up and the curve can cross the line of the operating frequency another time.

For sufficient RF efficiency the usual value is $|\beta_g| \approx (0.01 \div 0.02)$ which is not so far from the inversion curve. Suppose the operating point is chosen as $\Theta_0 = \frac{\pi}{3}, \beta_g = -0.01$, as it is shown in Fig. 20a. The dispersion curve behavior can be understood qualitatively by moving along a horizontal line $r = a_0$, Fig. 20a. Staring in direction of increasing Θ we are in the region of negative dispersion and the mode frequency decreases. At some Θ value we cross the inversion curve and the decrease of the frequency comes to an end. We enter the positive dispersion region and for further increase of Θ the mode frequency rises.

The simultaneous existence of two waves with different phase advance at the operating frequency is not tolerable both for RF and for beam dynamics reasons. In the classical DLW it can be

avoided only by limiting our choice of the operating point and restrict $\beta_g \leq -0.023$ for $\Theta_0 = \frac{\pi}{3}$, $\beta_g \leq -0.018$ for $\Theta_0 = \frac{\pi}{2}$ and $\beta_g \leq -0.01$ for $\Theta_0 = \frac{2\pi}{3}$ at the expense of the required RF power. For a SW mode the condition for the minimal value of $\Psi_{dm} \approx 2^\circ$ could be realized for $\frac{B}{A} = \frac{Z_0 h_{y0}}{e_{x0}} \approx -0.87$, [14], reflecting the minimal deviation of the central particle during bunch rotation, (53).

In general we can not derive a simple equation for the DS dispersion curve to understand the relative position of the point $\frac{B}{A} \approx -0.87$. According to the small pitch approximation for a DLW, from (19) the condition $\frac{B}{A} = -1.0$ corresponds to $k^2 a^2 = 2$, the condition $\frac{B}{A} \approx -0.87$ corresponds to $k^2 a^2 \approx 2.13$ and the inversion, (18), corresponds to $k^2 a^2 = 3$ or $\frac{B}{A} = -0.333$ (19). Results of simulations also show that a DS, which fulfills the condition of minimal Ψ_d , has a negative dispersion and a limited passband width $\sim (50 \div 70) MHz$, [14]. For the DLW SW case the dependence of the mode frequency on the aperture radius is plotted for different Θ in Fig. 21.

Due to the inversion phenomenon, the DS dispersion curve has not a classical 'cos' - like shape,

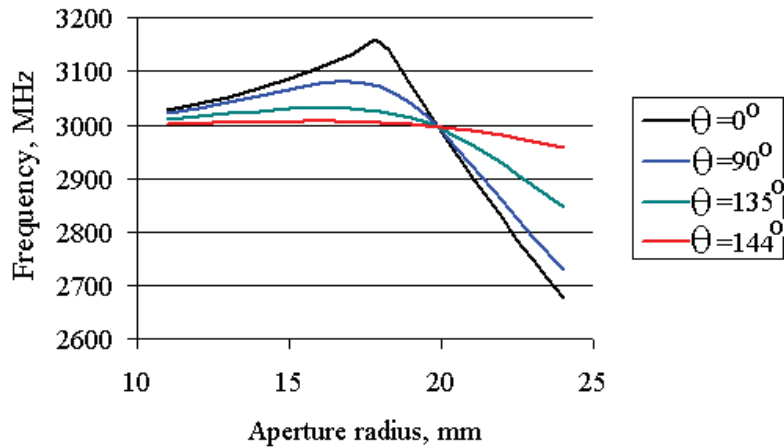


Figure 21: Plots of the mode frequency for the DLW SW case.

Fig. 20c, with very small frequency separation near the π mode. This provides a limitation either on the possible number of cells in the SW DS with minimized aberrations - the minimal value of Ψ_{dm} , or on the possible Ψ_d value.

To improve the frequency separation, the application of resonant slots is proposed in [14]. The resonant slots were also proposed for the stabilization of the deflecting plane [17]. One resonant slot with eigenfrequency $f_s \gg f_0$ is introduced into the disk to interact with the modes of the operating direction. The intensity of the slot excitation depends on both the value of f_s and of Θ of the cavity mode. The mode frequency shift, caused by the slots, $\delta f \sim \frac{(\sin \frac{\Theta}{2})^2}{f_s^2 - f_\pi^2}$, increases with Θ .

The slots result in $E_z \neq 0$ at the structure axis. To provide a larger δf with smaller slot excitation and reduced $E_z \neq 0$ at the deflector axis, the slots in adjacent disks should be rotated by π . The idea of the application of slots is to increase the negative slope of dispersion curve or to decrease the positive slope, Fig. 20 b, for $\Theta \approx \pi$ and relax, or remove in this way the limitations on choice of the DS parameters from the dispersion properties. For a practical realization this idea needs more detailed considerations.

10 Summary

In the beam aperture of deflecting structure the field distribution for the dipole mode can be described by linear combination of hybrid waves HE_1 and HM_1 . The deflecting field is composed from transverse components of electric and magnetic fields.

Only for the ultra relativistic case $\beta = 1$ is the synchronous spatial harmonic in the deflecting force free from non linear additions or aberrations. For lower particle energies even the synchronous harmonic has non linear additions, vanishing as $\frac{1}{\gamma^2\beta^2}$ in the distribution.

The sources of aberrations in the Lorenz force components are the higher spatial harmonics for the dipole mode and multipole additions. The multipole additions should be minimized in the development of the structure cross section. To estimate the relative level of spatial harmonics for the dipole mode components the criterion of maximal deviation of the field component phase from the phase of the synchronous harmonic is applied successfully.

For TW modes with low phase advance $\Theta_0 \leq \frac{\pi}{3}$ all structures have a relatively low level of spatial harmonics at the axis, both for the longitudinal and the transverse Lorenz force components. This is due to a strong attenuation of the harmonics from the aperture radius to the structure axis.

The level of aberrations in the E_d distribution strongly depends on the phasing and the balance of the hybrid waves HE_1 and HM_1 in the original field. For opposite phasing the synchronous harmonics in the transverse components of the electric and magnetic fields work for the deflection together, but higher harmonics compensate. For balanced amplitudes of the hybrid waves it leads to a strongly reduced level of higher harmonics in the E_d distribution, regardless of the level of harmonics in the original field components. This is also the only way to reduce aberrations in E_d strongly for SW modes, $\Theta_0 = \pi$, when the attenuation of harmonics in original field components is not sufficient.

For equal phasing of hybrid waves the level of spatial harmonics in E_d distribution is enlarged even as compared to the level of harmonics in original field components. In the motion of particles enlarged oscillations with respect to the line of deflection appear. In this case the bunch as a whole can be shifted to the outer region with an enlarged level of nonlinear additions in the field.

All structures with a pronounced predominance of the transverse electric field in the aperture have an equal phasing of hybrid waves.

Due to particularities in the hybrid wave distributions exists in DS's the phenomenon of the group velocity inversion. In most practical cases the opposite phasing results in a negative dispersion and a backward wave structure. The dispersion properties lead to limitations in the choice of structure parameters.

In a DLW structure the minimization of aberrations in E_d is possible at the expense of RF efficiency. Decoupling the control over magnetic and electric field distributions near the axis allows to combine both minimized aberrations and RF efficiency in the deflecting structure.

11 Acknowledgments

The author warmly thanks Dr. Klaus Floettmann, DESY, for support, discussion, beam dynamics expertise and for careful reading and correction of this paper.

This work was also supported in part by RBFR grant N 12 - 02 - 00654-a.

References

- [1] T.H. Fieguth, R.A. Gearhart, RF Separators and Separated Beams at SLAC, Proc. 1975 PAC, p. 1533
- [2] R. Akre, L. Bentson, P. Emma et. al., A Transverse RF Deflecting Structure for Bunch Length and Phase Space Diagnostic. Proc. 2001 PAC, p. 2353
- [3] G. Loew, R. Neal, Accelerating Structures, G. Dome, Review and Survey of Accelerating Structures, in Linear Accelerators, ed. P. Lapostolle, E. Septier, Amsterdam, 1970
- [4] V. Paramonov, L. Kravchuk, S. Korepanov. Effective standing wave RF structure for charged-particle beam deflector. Proc. Linac 2006 Conf., p. 469, 2006
- [5] Y. Garault, CERN 64-43, CERN, 1964
- [6] H. Hahn, Deflecting Mode in Circular Iris-Loaded Waveguides, Rev. Sci. Instr., v. 34, n. 10, p. 1094, 1963
- [7] J. Aleksandrov, V. Kotov, V. Vagin, P-2274, Dubna, 1975
- [8] W. Panofsky, W. Wenzel, Some Considerations Concerning the Transverse Deflection of Charged Particles in Radio-Frequency Fields. Rev. Sci. Instr., v. 27, p. 967, 1956
- [9] R.A. Silin, V.P. Sazonov, Slow wave systems, Sov. Radio, Moscow, 1966
- [10] P. Bernard et. al., CERN 68-30, D.Alesini et. al., CTTF3-003, INFN, Frascati, 2001
- [11] D. Malyutin et. al., Simulations of the longitudinal phase space measurements with the transverse deflecting structure at PITZ, Proc. IPAC 2012, p. 637, 2012
- [12] V. Paramonov, L. Kravchuk, The compensated periodical structure for RF deflector. Proc. Linac 2000 Conf., p.404, 2000
- [13] O.H. Altenmueller, R.R. Larsen, G.A. Loew, Investigations of Travelling-Wave Separators for the Stanford Two-Mile Accelerator, The Rev. of Sci. Instr., v. 35, n 4, 1964
- [14] V. Paramonov, K. Floettmann, L.V. Kravchuk, P. Orlov. Standing wave RF deflectors with reduced aberrations. Proc. RuPAC 2012, ISBN 978-3-954-50-125-0, p. 590, 2012
- [15] N. Kroll et al., Application of time domain simulations to coupler design for periodical structures. Proc. Linac 2000 Conf., p. 614, 2000
- [16] S. Minaev et.al., Electro-Dynamics Characteristics of RF Wobbler Cell for Heavy Ion Beam. Proc. 2010 LINAC Conf., p. 581
- [17] V. Paramonov, L. Kravchuk, The Resonant Method of Deflection Plane Stabilization. Proc. Linac 2010, p. 434.